

# From Internal Diagnosis to External Auditing: A VLM-Driven Paradigm for Online Test-Time Backdoor Defense

Binyan Xu<sup>1</sup> Fan Yang<sup>1</sup> Xilin Dai<sup>2</sup> Di Tang<sup>3</sup> Kehuan Zhang<sup>1</sup>

## Abstract

Deep Neural Networks remain inherently vulnerable to backdoor attacks. Traditional test-time defenses largely operate under the paradigm of internal diagnosis methods like *model repairing* or *input robustness*, yet these approaches are often fragile under advanced attacks as they remain entangled with the victim model’s corrupted parameters. We propose a paradigm shift from Internal Diagnosis to **External Semantic Auditing**, arguing that effective defense requires decoupling safety from the victim model via an independent, semantically grounded auditor. To this end, we present a framework harnessing Universal Vision-Language Models (VLMs) as evolving semantic gatekeepers. We introduce **PRISM** (Prototype Refinement & Inspection via Statistical Monitoring), which overcomes the domain gap of general VLMs through two key mechanisms: a *Hybrid VLM Teacher* that dynamically refines visual prototypes online, and an *Adaptive Router* powered by statistical margin monitoring to calibrate gating thresholds in real-time. Extensive evaluation across 17 datasets and 11 attack types demonstrates that PRISM achieves state-of-the-art performance, suppressing Attack Success Rate to  $< 1\%$  on CIFAR-10 while improving clean accuracy, establishing a new standard for model-agnostic, externalized security.

## 1. Introduction

Deep Neural Networks (DNNs) have achieved remarkable success in critical domains, yet they remain fundamentally vulnerable to *backdoor attacks* (Gu et al., 2019; Chen et al., 2017). By poisoning a small fraction of training data, adversaries implant hidden triggers that hijack model behavior on

<sup>1</sup>The Chinese University of Hong Kong, Hong Kong <sup>2</sup>Zhejiang University, China <sup>3</sup>Sun Yat-sen University, China. Correspondence to: Di Tang <tangd9@mail.sysu.edu.cn>, Kehuan Zhang <khzhang@ie.cuhk.edu.hk>.

Preprint. January 28, 2026.

specific inputs while preserving performance on benign data. The threat has rapidly evolved into an arms race: attacks have transitioned from conspicuous patterns to stealthy dynamic (Nguyen & Tran, 2020b), clean-label (Turner et al., 2019), and clean-image (Jha et al., 2024) strategies, making traditional detection increasingly difficult.

In Model-as-a-Service scenarios where defenders lack access to training data, test-time defense is the last line of defense. However, current research is constrained by the internal diagnosis paradigm, which exhibits fundamental vulnerabilities. (1) **Model Repairing Methods:** These methods attempt to identify backdoors by inspecting the victim model’s internal properties, such as neuron activation traces or Channel Lipschitzness (Zheng et al., 2022). While effective against static attacks, they rely on the assumption that backdoors leave conspicuous statistical footprints. Advanced dynamic attacks explicitly optimize triggers to suppress these internal anomalies, effectively bypassing such defenses. (2) **Input Robustness Methods:** These approaches, including input purification (Shi et al., 2023) and consistency checks (Liu et al., 2023), assume that triggers are sensitive to input perturbations or transformations. However, this assumption fails against *natural* backdoors (e.g., clean-image attacks using physical objects or filters), where the trigger is a robust, semantic feature inherent to the image, indistinguishable from benign features via perturbation. Consequently, a defense that remains robust across diverse attack modalities without relying on the compromised model’s internal states or fragile input assumptions remains an open challenge.

To overcome these limitations, we argue for a **paradigm shift**: moving from internal diagnosis to **Online External Semantic Auditing**. Instead of asking the compromised model to verify itself or testing the input’s robustness, we introduce an independent, “clean” agent to audit the prediction process. Universal Vision-Language Models (VLMs), such as CLIP (Radford et al., 2021) and Qwen-VL (Bai et al., 2025), offer the ideal foundation for this paradigm due to their vast, open-world semantic knowledge. By decoupling the defense mechanism from the victim model’s weights, we theoretically eliminate the attack surface exploited by weight-manipulation attacks.

While this paradigm holds immense promise, realizing its full potential requires addressing two key challenges: the **domain gap**, where VLMs underperform on specialized tasks compared to the victim model; and **threshold fragility**, where the semantic margin between correct and poisoned predictions varies drastically across samples, making static thresholding unreliable.

We propose PRISM (Prototype Refinement & Inspection via Statistical Monitoring), the first comprehensive framework for online external semantic auditing. PRISM wraps the victim model in a dual-stream architecture, employing the VLM not merely as a classifier, but as an evolving *semantic gatekeeper*. (1) To bridge the domain gap, we design a **Hybrid VLM Teacher** that augments static text anchors with visual prototypes learned *online* from the test stream. This allows the auditor to adapt to the specific feature distribution of the task without offline training. (2) To address threshold fragility, we introduce an **Adaptive Router** powered by *online statistical monitoring*. By modeling the logit margin distribution using the Cornish-Fisher expansion, PRISM continuously calibrates the auditing sensitivity, ensuring robustness against distribution shifts.

Our evaluation across 17 datasets and 11 SOTA attacks confirms the superiority of this new paradigm. PRISM effectively neutralizes attacks that bypass model repair and input purification methods, such as clean-image and adaptive flooding attacks. It consistently suppresses the Attack Success Rate (ASR) to  $< 1\%$  on CIFAR-10 while even improving Clean Accuracy. PRISM establishes that decoupling defense through external semantic auditing is not only feasible but essential for next-generation model security.

Our main contributions are summarized as follows:

- **New Paradigm (External Semantic Auditing):** We identify failure modes of internal diagnosis paradigms and propose a novel direction that uses universal VLMs as independent, external auditors, effectively decoupling defense from compromised victim models.
- **Online Adaptive Framework (PRISM):** We propose PRISM <sup>1</sup>, a test-time framework that turns generic VLMs into effective auditors. With a *Hybrid VLM Teacher* and an *Adaptive Router*, we bridge the domain gap and avoid static thresholds via online adaptation and statistical monitoring.
- **Superior Generalization and Robustness:** PRISM achieves state-of-the-art performance across 17 datasets and 6 VLM backbones. It demonstrates unique robustness against advanced clean-image and adaptive attacks where traditional paradigms fail, setting a new standard for model-agnostic defense.

<sup>1</sup><https://anonymous.4open.science/r/PRISM-552>

## 2. Related Work

### 2.1. Vision-Language Models (VLM)

**Vision-Language Embedding Models.** These models bridge modalities by embedding large-scale data into a shared feature space, simultaneously learning visual and textual representations. CLIP (Radford et al., 2021), a seminal VLE model, achieves strong generalization by training on a 400M image-text dataset, treating paired images and texts as positives and all others as negatives.

**Vision-Language Generative Models.** Large Vision-Language Models (LVLMs) extend Large Language Models (LLMs) with visual understanding capabilities. Open-source models like LLaVA (Liu et al., 2024) connect vision encoders with LLMs via projection layers for visual instruction tuning. More recent advancements include Qwen-2.5-VL (Bai et al., 2025), which excels in high-resolution processing, and Gemma-3 (Team et al., 2025), which adopts a native multimodal architecture. Despite their growing popularity, their potential in enhancing model security, particularly for defending against backdoors, has not been investigated.

**VLM for Security.** Most existing works on VLM focus on security concerns of VLM itself, such as backdoor attacks (Liang et al., 2024), adversarial attacks (Xu et al., 2025a), and pre-training defenses (Yang et al., 2024). The application of VLMs in defending other models remains underexplored. Limited exceptions use CLIP for training-time dataset cleansing (Xu et al., 2025b) or for mitigating backdoors in Federated Learning via prototype alignment (Gai et al., 2025). In distinct contrast, our method addresses a more practical and challenging scenario, representing the first use of VLM for test-time backdoor defense without requiring training interventions or access to model weights.

### 2.2. Backdoor Attacks and Defenses

#### 2.2.1. BACKDOOR ATTACKS.

Backdoor attacks are often implemented via data poisoning (Gu et al., 2019; Chen et al., 2017; Barni et al., 2019), where adversaries inject poison samples into the training dataset, causing the victim model to associate backdoor triggers with target classes. Beyond data poisoning, backdoor attacks can also manipulate the training process (Nguyen & Tran, 2020b;a; Wang et al., 2022), though these can be adapted into data poisoning by introducing additional noise samples (Wu et al., 2024). Some attacks use benign images as backdoor triggers (Jha et al., 2024; Xu et al., 2025c) to evade detection.

#### 2.2.2. TEST-TIME BACKDOOR DEFENSES.

**Model Repairing Methods** aim to remove backdoors from a compromised model by modifying model weights. Some approaches use model-intrinsic properties, such as Channel Lipschitzness Pruning (CLP) (Zheng et al., 2022) and its

improved version LPP (Wang et al., 2025), which prune neurons based on sensitivity differences. Others, like C&C (Phan et al., 2024), utilize model compression techniques to destroy fragile backdoor correlations. Additionally, methods like BCU (Pang et al., 2023) assume access to a set of unlabeled data to purify the model via self-supervised learning. While our method also operates without labeled training data, it distinctively employs an online learning paradigm during testing, continuously adapting to the input stream rather than performing a one-time static repair.

**Input Robustness Methods** focus on identifying or mitigating backdoored inputs with robustness measures during the inference stage. SCALE-UP (Guo et al., 2023) and TeCo (Liu et al., 2023) detect triggers by analyzing prediction consistency under input scaling or corruption. BDMAE (Sun et al., 2023) and ZIP (Shi et al., 2023) employ pretrained generative models (MAE and Stable Diffusion) for zero-shot image purification to remove trigger patterns. More recently, REFINE (Chen et al., 2025) utilizes model reprogramming to learn visual prompts that neutralize backdoors. Although our approach falls into this category, it differs fundamentally from prior works by introducing an *online* mechanism. We are the first to combine the semantic power of Universal VLMs with online statistical monitoring to dynamically refine the defense strategy test-time, offering superior adaptability and robustness.

### 3. Preliminary

#### 3.1. Notations.

We consider a classification model  $f(\cdot; \theta)$  parameterized by  $\theta$ . Let  $\mathcal{X}$  denote the input space. Let  $p(y | x; \theta)$  denote the predicted probability assigned by the model  $f(\cdot; \theta)$  to class  $y$  given input  $x$ . The predicted label for  $x$  is then defined as

$$\hat{y}(x) = \arg \max_{y \in \mathcal{Y}} p(y | x; \theta),$$

where  $\mathcal{Y} = \{1, 2, \dots, C\}$  is the set of possible class labels. We define the trigger function as  $\mathcal{T} : \mathcal{X} \rightarrow \mathcal{X}$ , and let  $y_t \in \mathcal{Y}$  represent the attack’s designated target class.  $\mathcal{P}$  denotes the distribution of clean, unaltered samples. The clean accuracy (CA) of the model is the probability of correct classification on clean data,  $\mathbb{P}_{(x,y) \sim \mathcal{P}}[\hat{y}(x) = y]$ . The attack success rate (ASR),  $\mathbb{P}_{(x,y) \sim \mathcal{P}|y \neq y_t}[\hat{y}(\mathcal{T}(x)) = y_t]$ , measures the probability that a sample  $x$  with a trigger is misclassified as the target class  $y_t$ .

#### 3.2. Threat Model.

We adopt a stringent test-time threat model where the defender deploys a potentially compromised “suspicious model”  $f_S$  without access to its original training data. The adversary may have embedded arbitrary backdoors—including stealthy clean-label or dynamic triggers—into  $f_S$ . To secure the inference, the defender utilizes a public, pre-trained, and clean VLM as an external au-

ditor. As a foundation model pre-trained on billion-scale open-world corpora, the VLM’s feature space is statistically independent to the specific, poisoned distribution of the victim, making it blind to local triggers. Furthermore, the VLM remains strictly frozen during the defense phase, eliminating the attack surface for test-time weight manipulation. The defense goal is to purify the prediction stream online, minimizing ASR while preserving CA.

## 4. Methodology

### 4.1. Overview of PRISM

To secure deployed models against diverse backdoor attacks without accessing training data, we propose **PRISM** (Prototype Refinement & Inference via Statistical Margin). As illustrated in Fig. 1, PRISM functions as a test-time wrapper around the suspicious victim model. The core intuition is that while backdoor triggers force the victim model to output high-confidence predictions on poisoned samples, these predictions often lack semantic support in the feature space of a benign, general-purpose Vision-Language Model (VLM). PRISM exploits this semantic discrepancy through a three-pillar architecture: (1) A **Dual Stream Inference** framework that processes inputs through both the victim model and a trusted Universal VLM Teacher; (2) A **Hybrid VLM Teacher** that enhances zero-shot capabilities by fusing static text anchors with dynamically refined visual prototypes; and (3) An **Adaptive Router** that employs online statistical monitoring to gate predictions based on a difficulty-aware logit margin. By continuously updating the statistical moments and visual prototypes using Cumulative Moving Average (CMA), PRISM adapts to the test stream distribution in an online manner, effectively filtering out backdoor triggers while preserving benign performance.

### 4.2. Dual Stream Inference Framework

The foundation of PRISM is a parallel inference mechanism designed to decouple the potential risk from the decision process. For any incoming test sample  $x$ , the system initiates two concurrent forward passes. The first stream passes  $x$  through the suspicious model  $f_S$ , yielding a prediction  $\hat{y}_S$  and its associated logits. While  $f_S$  is potentially compromised, it typically possesses high domain-specific utility. The second stream processes  $x$  through a frozen, trusted VLM backbone. Unlike prior works that rely solely on static zero-shot classification, which may suffer from domain shifts, our framework treats the VLM as a “Universal Teacher” that provides a semantic verification signal. The outputs of these two streams—the suspicious logits from the victim and the robust logits from the hybrid VLM—are then fed into the Adaptive Router. This dual-stream design ensures that the system defaults to the high-performance victim model for benign samples but falls back to the robust VLM prediction when a backdoor attack is detected.

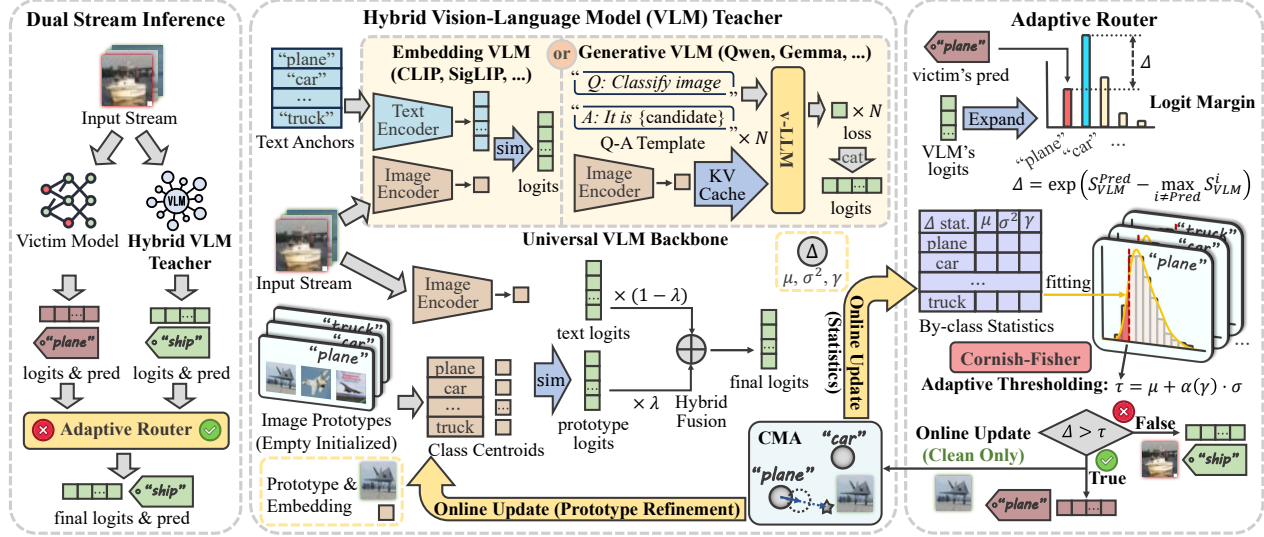


Figure 1. Pipeline of PRISM (Prototype Refinement &amp; Inspection via Statistical Monitoring).

### 4.3. Universal Hybrid VLM Teacher

A critical limitation of using standard VLMs for defense is their variable zero-shot performance on specialized downstream tasks. To address this, we introduce a Universal VLM Backbone that supports both embedding-based models (e.g., CLIP, SigLIP) and generative models (e.g., Qwen, Gemma), enhanced by a hybrid anchoring mechanism.

**Universal Backbone Support.** For embedding-based VLMs, we compute the cosine similarity between the image embedding  $z_{img}$  and the text embeddings  $z_{text}$  of the candidate class labels. For generative VLMs, which are typically computationally intensive, we optimize inference using a Key-Value (KV) Cache strategy. We construct a prompt template  $Q$ : “Classify this image”, and evaluate the probability of the model generating specific class names as answers. By caching the visual features and the system prompt’s hidden states, we avoid redundant computations for the invariant parts of the input. The classification logits are derived from the language modeling loss associated with each candidate label token, effectively converting the generative output into a discriminative probability distribution.

**Hybrid Anchors: Text and Prototypes.** To bridge the gap between general semantic knowledge and task-specific feature distributions, we employ a hybrid fusion strategy. While static text anchors provide high-level semantic guidance, they often fail to capture fine-grained intra-class variance. We therefore augment the auditor with dynamic visual prototypes (k-class centroids), denoted as  $\mathcal{C} = \{c_1, \dots, c_K\}$ . Specifically, given the normalized image embedding  $z_{img}$  of an incoming test sample, we compute two distinct logit sets: (1)  $S_{text}$ , derived from the cosine similarity between  $z_{img}$  and the predefined text anchors  $\mathcal{T}$ ; and (2)  $S_{proto}$ , calculated as the similarity between  $z_{img}$  and the current class centroids  $\mathcal{C}$ . Crucially, to adhere to our data-free constraint,

$\mathcal{C}$  is initialized and refined online using samples from the test stream (detailed in Sec. 4.5). The final VLM logits  $S_{VLM}$  are obtained via the weighted fusion:

$$S_{VLM} = \lambda \cdot \underbrace{\text{Sim}(z_{img}, \mathcal{C})}_{S_{proto}} + (1 - \lambda) \cdot \underbrace{\text{Sim}(z_{img}, \mathcal{T})}_{S_{text}}, \quad (1)$$

where  $\lambda$  is a balancing coefficient. This formulation allows the VLM teacher to use broad linguistic semantics while adapting to the specific visual manifold of the test stream.

### 4.4. Adaptive Router via Statistical Monitoring

Adaptive Router is the core decision logic of PRISM, which determines whether to accept the victim model’s prediction or reject it in favor of the VLM. This decision is governed by a statistical discrepancy test based on logit margins.

**Logit Margin Calculation.** We define a discrepancy metric  $\Delta$  that quantifies the semantic support the VLM provides for the victim model’s prediction  $\hat{y}_S$ . We examine the VLM’s logits  $S_{VLM}$  specifically at the index  $\hat{y}_S$  and compare it to the maximal logit of all other classes  $i \neq \hat{y}_S$ . The logit margin  $\Delta$  is formally defined as:

$$\Delta = \exp \left( S_{VLM}^{\hat{y}_S} - \max_{i \neq \hat{y}_S} S_{VLM}^i \right) \quad (2)$$

We employ the exponential transformation to ensure statistical stability. Since raw logit differences are unbounded and can approach  $-\infty$  when the VLM strongly rejects the victim’s prediction, the exponential mapping suppresses these extreme negative outliers, confining the metric to a robust positive range. Consequently, a small  $\Delta$  (near 0) implies strong disagreement, while a large  $\Delta$  indicates alignment.

**Adaptive Thresholding via Cornish-Fisher Expansion.** A static threshold for  $\Delta$  is insufficient due to the non-Gaussian, often skewed nature of the discrepancy distribution (empirical validation in App. ??). To address this, we model the

distribution of  $\Delta$  for each class  $k$  online, maintaining the running statistics of mean  $\mu_k$ , standard deviation  $\sigma_k$ , and skewness  $\gamma_k$ . We employ the Cornish-Fisher expansion to derive an adaptive threshold  $\tau_k$ , which approximates the quantiles of a non-Gaussian distribution (derived in App. A). Let  $\zeta$  denote the base confidence coefficient. The skewness-adjusted coefficient  $\tilde{\zeta}_k$  is calculated as:

$$\tilde{\zeta}_k = \zeta + \frac{\gamma_k}{6}(\zeta^2 - 1). \quad (3)$$

This correction term shifts the threshold to account for asymmetry: positive skewness raises the threshold to reduce false rejections, while negative skewness lowers it. The final adaptive threshold is defined as  $\tau_k = \mu_k + \tilde{\zeta}_k \cdot \sigma_k$ . If the discrepancy  $\Delta$  of a test sample exceeds  $\tau_k$ , it is deemed consistent and accepted.

#### 4.5. Online Update and Prototype Refinement

To address statistical instability during the initial “cold start” phase, PRISM employs *progressive confidence weighting*. We initialize the router with a *conservative Gaussian prior* (assuming skewness  $\gamma = 0$ ) and linearly interpolate to the skewness-aware Cornish-Fisher correction as the sample count accumulates ( $N \approx 100$ ). This ensures statistical stability before activating the full adaptive mechanism.

After warm-up, we apply a feedback loop that updates internal states only when a sample is certified as clean (i.e.,  $\Delta > \tau$ ). Crucially, to ensure robustness against temporal distribution shifts, we employ Cumulative Moving Average (CMA) rather than Exponential Moving Average (EMA). Unlike EMA, which is susceptible to local drift, CMA provides statistical inertia, ensuring that the global distribution estimate becomes increasingly stable over time. Furthermore, this update process is designed for memory efficiency; we strictly update statistical moments  $(\mu, \sigma, \gamma)$  and class feature centroids  $(c_k)$  in place without retaining a replay buffer of raw images, thereby minimizing computational overhead to  $O(1)$  (algorithm details in App. B).

## 5. Evaluation

### 5.1. Experiment Setup

**Attack Baselines.** We evaluate PRISM against 11 SOTA backdoor attacks in four categories: *Classic* (BadNets (Gu et al., 2019), Blend (Chen et al., 2017)); *Dynamic* (SSBA (Li et al., 2021), IAB (Nguyen & Tran, 2020a), WaNet (Nguyen & Tran, 2020b), BPP (Wang et al., 2022)); *Clean-Label* (LC (Turner et al., 2019), SIG (Barni et al., 2019), CTRL (Li et al., 2023)); *Clean-Image* (FLIP (Jha et al., 2024), GCB (Xu et al., 2025c)). We set target label  $y_t=0$ , using a 50% poison rate for clean-label attacks and 5% otherwise (full config in App. D).

**Defense Baselines.** PRISM is compared against 8 recent SOTA defenses: (1) *Model repairing*: CLP (Zheng et al., 2022), C&C (Phan et al., 2024), LPP (Wang et al., 2025); (2)

*Input robustness*: ScaleUp (Guo et al., 2023), ZIP (Shi et al., 2023), TeCo (Liu et al., 2023), BDMAE (Sun et al., 2023), Refine (Chen et al., 2025), with configuration from BackdoorBench (Wu et al., 2022) or their official repositories. We also have two VLM baselines: *Zero-shot*, which directly uses VLMs for classification; and *Ensemble*, which averages the logits of the victim model and VLM for prediction.

**PRISM Configuration.** We evaluate PRISM across diverse VLMs, including embedding models (CLIP (Radford et al., 2021), SigLIP (Zhai et al., 2023), ImageBind (Girdhar et al., 2023)) and generative models (Qwen2.5-VL-7b (Bai et al., 2025), LLaVA-1.5-7b (Liu et al., 2024), Gemma3-4b (Team et al., 2025)), all using official pre-trained weights. Unless otherwise specified, we set the base adaptive threshold  $\zeta = -2$ , victim model to PreActResNet18, Auditing VLM to CLIP, batch size to 256, and prototype fusion weight  $\lambda_p = 0.5$ . For warm-up, we use the initialization window  $N$  of only one batch of unlabeled images.

**Datasets.** Our evaluation spans 17 datasets categorized into: (1) *General Datasets* (e.g., CIFAR-10, CIFAR-100, ImageNet), and (2) *Domain-Specific Datasets* (e.g., MNIST, GTSRB, Texture datasets). The latter poses a significant challenge, as general VLMs often exhibit significant performance gaps compared to specialized victim models (e.g., 40% VLM accuracy vs. 95% victim accuracy on MNIST).

**Evaluation Metrics.** We report Clean Accuracy (CA) and Attack Success Rate (ASR). An ideal defense should minimize ASR to near-zero levels while maintaining a CA comparable to the original model.

### 5.2. Main Results

#### 5.2.1. PRISM vs. BASELINES.

**Performance Superiority.** PRISM significantly outperforms all existing data-free and test-time baselines. As detailed in Table 1, PRISM is the sole method capable of suppressing ASR below 15% across all 11 attack types while simultaneously improving Clean Accuracy (CA) on CIFAR-10. Existing SOTA methods exhibit severe vulnerabilities: defenses like CLP and ScaleUp fail completely against Clean-Image backdoors (FLIP, GCB), while ZIP and TeCo struggle with Dynamic attacks. Notably, the strongest baseline, Refine (Chen et al., 2025), fails to defend against Clean-Image attacks. While the naive Zero-shot VLM baseline achieves low ASR, it incurs catastrophic CA drops (e.g.,  $\geq 70\%$  drop on GTSRB), rendering it impractical. PRISM successfully bridges this gap, offering comprehensive protection without compromising utility.

**Overhead Efficiency.** Fig. 2 illustrates the runtime performance on an NVIDIA A100 GPU with a batch size of 1. PRISM (CLIP) shows high efficiency, ranking as high as 2nd among defenses with an inference latency of 12.5 ms per image. While large generative backbones (e.g., Qwen)

**Table 1. Comparative evaluation of backdoor defenses on CIFAR-10.** ASRs below 15% are highlighted in blue (success), while those above 15% are in red (failure). PRISM is the only method that successfully defends against all 11 attack types while maintaining high Clean Accuracy (CA), whereas existing SOTA defenses fail significantly on Clean-Image backdoors (FLIP, GCB) or Dynamic attacks.

Defense →	No Defense		Existing Backdoor Defenses								Naive VLM Baselines		PRISM (Ours)		
	CA	ASR	CA	ASR	CA	ASR	CA	ASR	CA	ASR	CA	ASR	CA	ASR	
Attack ↓	CA	ASR	CA	ASR	CA	ASR	CA	ASR	CA	ASR	CA	ASR	CA	ASR	
Classic	BadNet	92.3	87.9	90.7	12.4	90.2	0.2	90.0	0.1	86.4	9.1	92.4	26.4	90.3	
	Blend	93.6	99.4	90.3	76.3	84.1	97.5	91.6	73.4	87.3	5.7	83.8	0.8	84.7	50.7
Dynamic	WaNet	91.1	94.1	89.1	2.0	76.2	89.2	89.5	9.7	45.6	70.9	92.0	99.0	91.1	94.0
	BPP	91.5	99.4	91.2	1.7	85.3	0.4	88.5	38.0	83.8	2.2	88.7	10.9	90.4	86.1
	IAB	91.5	95.0	91.1	4.5	82.9	2.3	89.8	40.5	82.3	61.3	80.8	7.9	86.0	25.4
	SSBA	93.0	97.3	90.7	42.8	83.7	0.0	91.5	15.3	88.1	10.4	84.3	4.5	84.0	13.0
Clean Label	CTRL	93.6	95.9	91.7	0.9	82.4	43.1	92.1	19.7	88.3	1.6	85.3	11.8	93.1	95.3
	SIG	93.6	93.9	90.3	93.5	84.5	79.3	92.3	79.9	90.0	97.3	83.5	6.2	85.7	34.6
	LC	93.4	98.4	87.4	18.4	88.2	0.0	92.8	0.0	89.7	1.0	84.2	7.2	85.4	30.9
Clean Image	FLIP	89.9	99.2	89.1	28.5	81.5	0.1	88.3	94.5	86.5	87.6	85.3	50.0	87.3	69.1
	GCB	88.6	100.	89.1	100.	81.5	100.	85.6	100.	78.7	100.	88.9	100.	90.2	69.4
Average		92.0	96.4	90.1	34.6	83.7	37.5	90.2	42.8	82.4	40.6	86.3	29.5	87.7	55.3
CA Drop (smaller is better)		▼1.9	▼8.3	▼1.8	▼9.6	▼5.7	▼4.3	▼2.7	▼5.1	▼5.3	▼4.7	▼5.7	93.2	0.8	▲2.7
ASR Drop (larger is better)		▼61.8	▼58.9	▼53.6	▼55.8	▼66.9	▼41.1	▼67.6	▼82.1	▼96.0	▼20.7	▼95.6			▲1.2

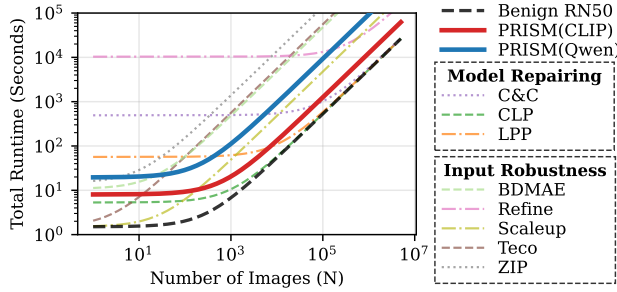


**Figure 2. Inference Latency comparison for all test-time defenses on ImageNet.** PRISM (CLIP version) ranks 2/9 at best and ranks 4/9 at worst among all the tested methods.

will incur higher latency compared to embedding models, our extensive evaluations confirm that the lightweight CLIP auditor achieves sufficient defense performance, making the additional computational cost of generative models unnecessary for most practical deployment scenarios.

### 5.3. Robustness Evaluation

#### 5.3.1. ROBUSTNESS ACROSS VLM ARCHITECTURES.

PRISM exhibits strong robustness to VLM architectural variations. As shown in Fig. 4, whether using embedding models (CLIP, SigLIP) or generative models (Qwen, LLaVA), PRISM consistently limits ASR to below 10% across both general and domain-specific datasets (expanded results in App. M). A *counter-intuitive observation* is that PRISM maintains high CA even when VLM’s zero-shot accuracy is poor (e.g., on GTSRB). Conversely, when zero-shot accuracy is higher (e.g., ImageBind on TinyImageNet), PRISM can even repair CA to match superior zero-shot performance. This phenomenon occurs because our *Adaptive Router* effectively decouples defense capability from VLM performance: in low-performance domains, the VLM acts as a weak constraint that only intercepts high-confidence statistical outliers (triggers), while deferring to the victim model’s superior domain knowledge for benign samples. For specialized domains like healthcare and backdoored VLMs, we further explore a ‘Trust Chain’ strategy in App. F.

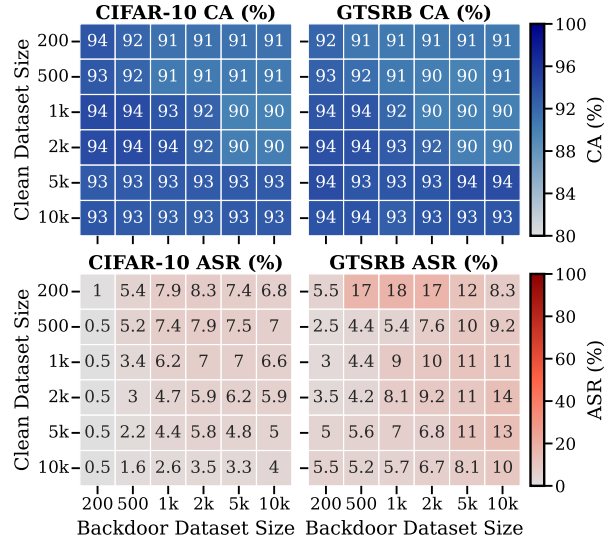


**Figure 3. Scalability to Dataset Size.** PRISM maintains stable performance (CA variation < 4%, ASR < 20%) across datasets ranging from 200 to 10,000 images, demonstrating robustness to the scale of the inference stream.

#### 5.3.2. DATASET SIZE SCALABILITY.

PRISM demonstrates robustness across dataset sizes varying by three orders of magnitude. Figure 3 shows that ASR is consistently suppressed below 20% across all scales. We observe a performance pattern related to the ratio of poisoned to clean samples (upper triangle region): when the number of backdoor samples significantly exceeds clean samples, performance slightly degrades. This is expected, as the online statistical monitoring is influenced by the dominant data mode. However, even in extreme scenarios where the poison set is 50× larger than the clean set, ASR remains effectively controlled at ~ 12%, validating the inertia and robustness of our CMA-based online update mechanism.

#### 5.3.3. DATASET SCALABILITY.

Table 2 validates PRISM across 17 datasets with varying scales and Imbalance Ratios (IR, defined as the ratio of

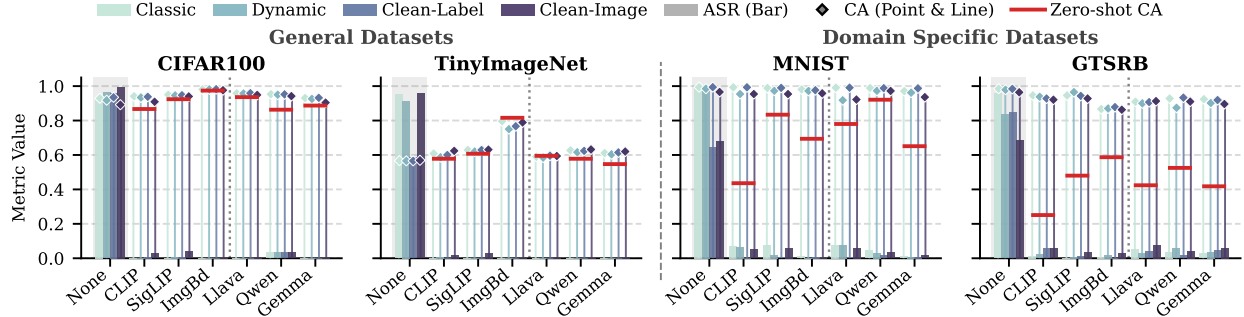


Figure 4. Robustness across VLM Architectures. PRISM consistently reduces ASR to < 8% across 6 different VLMs (Embedding & Generative). It maintains CA drops within 5%, even on domain-specific datasets (GTSRB) where baseline VLM performance is low.

Table 2. Scalability across 17 datasets with different Imbalance Ratio (IR). PRISM successfully defends against all tested attacks (Blend, BPP, CTRL) across all datasets.

Dataset ↓	IR	Accuracy		Blend		BPP		CTRL	
		VLM	RN50	ΔCA	ASR	ΔCA	ASR	ΔCA	ASR
SVHN	3.20	13.4	95.5	▼1.6	0.8	▼1.9	1.6	▼1.8	1.8
Country211	1.00	17.2	6.8	▲5.3	0.0	▲5.4	1.4	▲5.3	0.0
GTSRB	12.5	25.1	97.8	▼4.9	2.5	▼0.7	0.0	▼5.9	6.7
FER2013	16.0	41.4	63.0	▼5.6	0.0	▼3.8	4.8	▼4.7	4.8
DTD	1.00	43.6	99.5	▼0.3	6.7	▲0.0	3.3	▼0.3	0.0
TinyImgNet	1.00	44.3	25.7	▲17.8	0.0	▲16.3	0.0	▲19.6	0.0
StanfordCars	2.83	57.8	57.2	▲1.9	0.0	▼0.9	0.0	▼1.8	0.0
ImageNet	1.00	59.6	49.3	▲9.9	0.0	▲13.8	2.5	▲5.4	0.0
SUN397	37.7	62.2	66.1	▼1.2	2.0	▼1.2	0.0	▼2.1	0.0
MNIST	1.00	62.3	69.2	▲2.2	0.0	▲3.4	0.0	▲1.0	0.0
CIFAR100	1.00	62.5	55.3	▲12.9	0.9	▲14.2	0.9	▲13.0	0.9
Flowers102	1.00	66.5	31.0	▲15.2	0.0	▲12.7	0.0	▲17.7	0.0
Caltech101	86.5	81.6	68.8	▲12.7	0.0	▲14.1	0.0	▲11.3	0.0
CIFAR10	1.00	86.7	92.9	▲0.5	0.0	▲2.3	1.1	▲0.6	0.0
OxfordIIITPet	1.14	87.3	26.6	▲1.9	2.9	▲5.4	2.9	▲4.5	2.9
Food101	1.00	88.8	68.7	▲8.9	1.6	▲10.9	0.0	▲14.1	0.0
STL10	1.00	97.1	64.8	▲33.4	1.4	▲33.0	0.0	▲26.2	0.0

samples in the majority class to the minority class). The method proves robust against extreme imbalance (e.g., Caltech101, IR=86.5) and does not rely on high VLM performance. For instance, despite a low zero-shot accuracy of 13.4% on SVHN, PRISM remains effective (See App. K for TPR/FPR analysis). This implies that even imperfect VLM signals are sufficient to identify trigger-induced statistical anomalies distinct from natural data manifolds.

### 5.3.4. POISON RATE ROBUSTNESS.

Unlike many defenses that are sensitive to poison rates (Zheng et al., 2022), PRISM exhibits strong robustness due to its reliance on semantic logit similarity rather than intrinsic model properties. PRISM controls CIFAR-10 ASR to  $\leq 5\%$  and GTSRB ASR to  $\leq 12\%$  across all poison rates (1%, 5%, 10%), demonstrating high practical reliability (additional rates in App. L).

## 5.4. Ablation Study

### 5.4.1. COMPONENT ANALYSIS

We conduct an ablation study to quantify the contribution of three core components: Online Update, Prototype Refinement, and Skewness Correction. Table 3 summarizes the results (full breakdown in App. N). (1) **Online Update**: This

Table 3. Component Ablation Study. Impact of removing Online Update, Prototype Refinement, and Skewness Correction. Best results under each case are presented with optimal hyperparameters.

Ablation Cases →	Baseline		w/o Online		w/o Prototype		w/o Skewness	
	CA	ASR	CA	ASR	CA	ASR	CA	ASR
CIFAR100								
Classic	72.8	▲2.3	0.0	71.5	▲1.0	5.7	71.0	▲0.5
Dynamic	70.4	▲4.5	0.0	70.4	▲4.5	4.0	69.7	▲3.8
C-Label	73.2	▲2.5	0.0	72.0	▲1.4	5.1	71.1	▲0.5
C-Image	69.1	▼1.0	1.0	69.0	▼1.2	6.3	68.9	▼1.3
GTSRB								
Classic	94.4	▼4.1	1.3	90.3	▼8.2	32.9	86.1	▼12.4
Dynamic	92.1	▼5.8	2.1	87.9	▼10.	21.0	86.1	▼11.8
C-Label	92.5	▼5.9	5.8	88.2	▼10.	31.1	83.2	▼15.3
C-Image	90.3	▼6.1	4.5	85.3	▼11.	8.6	80.5	▼16.0

is crucial for adaptation. Without online updates, PRISM fails on domain-specific datasets like GTSRB (ASR spikes to  $\sim 40\%$ ). This failure stems from the inherent bias in pre-trained VLMs; static gating propagates this bias, whereas online adaptation corrects it. (2) **Prototype Refinement**: This component significantly impacts Clean Accuracy, particularly on specialized domains. For instance, removing prototypes causes a CA drop of nearly 20% on GTSRB, rendering the defense too costly in terms of utility. (3) **Skewness Correction**: While the aggregated results appear stable, this stability assumes optimal hyperparameter tuning. As shown in Figure 5, PRISM achieves global optimality at  $\zeta = -2$  across all datasets. In contrast, without Skewness Correction (i.e., assuming a Gaussian distribution), the optimal threshold varies wildly across datasets (e.g., -2 for CIFAR vs. -3 for GTSRB), making deployment impractical. Skewness Correction effectively standardizes the distribution, allowing for a uniform hyperparameter configuration.

### 5.4.2. HYPERPARAMETER ANALYSIS

We analyze the base threshold coefficient  $\zeta$ . Results across two VLM backbones and four datasets confirm that  $\zeta = -2$  is consistently optimal. This value is not arbitrary but aligns with statistical theory: in a standard normal distribution,  $\mu - 2\sigma$  covers  $\approx 95\%$  of the probability mass. Our skewness correction effectively maps the skewed margin distribution to this standard form, allowing the  $\zeta = -2$  setting to serve as a robust, theoretically grounded default that generalizes across diverse attack and data landscapes (see Figure 5).

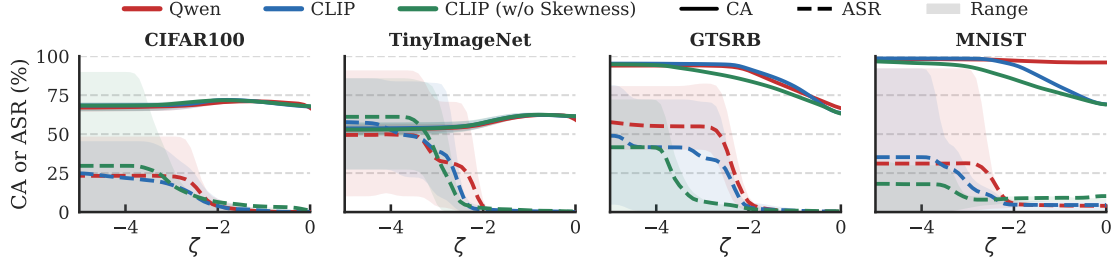


Figure 5. Hyperparameter Sensitivity of  $\zeta$ . PRISM reaches optimal performance consistently at  $\zeta = -2$  across all datasets and attacks. Without Skewness Correction, the optimal threshold fluctuates significantly between datasets, validating the necessity of our Cornish-Fisher expansion for robust, dataset-agnostic deployment.

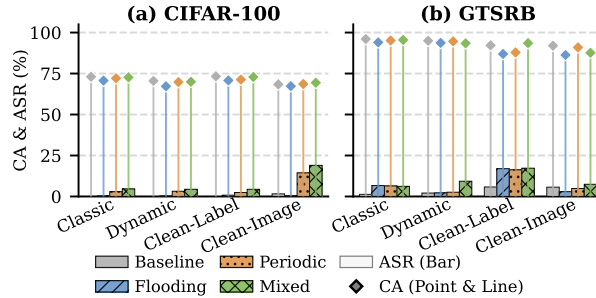


Figure 6. Robustness against Adaptive Attacks. ASR remains below 20% against 3 types of online adaptive attacks (Flooding, Periodic, Mixed), proving the resilience of the update mechanism.

## 5.5. Adaptive Attacks

We evaluate PRISM against adaptive adversaries aware of our defense strategy, considering both online manipulation and semantic evasion.

### 5.5.1. ONLINE ADAPTIVE ATTACKS

We synthesize three adaptive online strategies: (1) *Flooding*, where backdoor samples dominate the stream ( $> 90\%$ ); (2) *Periodic*, employing alternating waves of clean and poisoned data; and (3) *Mixed*, injecting poison from the very start to corrupt the initialization. As shown in Figure 6 and 7, PRISM remains robust against all three strategies (ASR  $< 20\%$ , CA drop  $< 5\%$ ). This resilience is attributed to our **Selective**

**Update Mechanism:** the system only updates statistics using samples that pass the gate ( $\Delta > \tau$ ). Consequently, flooding attacks are rejected and do not corrupt the internal state. Similarly, for mixed attacks, the statistical inertia provided by the CMA mechanism ensures that minor initial impurities do not destabilize the defense trajectory.

### 5.5.2. AUDITOR-AWARE ADAPTIVE ATTACKS

To rigorously stress-test the “trusted auditor” assumption, we evaluate PRISM against semantic typography attacks

designed to mislead the VLM. We explicitly exclude visually semantic-consistent triggers from this setting (e.g.: add dog’s feature to make images classified as a dog). Such triggers fundamentally alter the visual ground truth of the input, violating the definition of a backdoor attack (where the input should not semantically belong to the target class). Thus, we focus on textual triggers which induce semantic shortcuts without overriding visual features.

As shown in Fig. 9, we superimpose target class names (e.g., “Plane”) onto benign images (setup details in App. H). Results in Table 4 reveal that this attack compromises the standalone VLM, raising zero-shot ASR to 60.1%. While freezing the VLM eliminates parameter-level tampering, we acknowledge that the *input surface* remains susceptible to semantic manipulation, as evidenced by PRISM’s ASR rising to 15.6%.

However, PRISM still suppresses the attack significantly compared to the unprotected VLM. This shows that even when the VLM’s textual alignment is bypassed, PRISM’s *online visual prototype refinement* provides a critical safety layer by detecting the distributional discrepancy between the typographic attack and authentic target samples. Additional feature mixing attacks are discussed in App. I.

Table 4. Defense against adaptive text prompt attack.

	Zero-shot	PRISM
Prompt Attack	CA ASR	CA ASR
Original	86.7 0.2	92.3 1.3
Adaptive	86.7 60.1	92.2 15.6

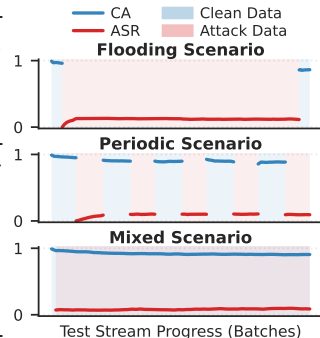


Figure 7. Online Attack Stream Analysis on GTSRB. The defense remains effective throughout the iteration stream.

## 6. Conclusion

We present PRISM, a pioneering test-time defense framework re-defining backdoor mitigation via online external semantic auditing. Harnessing Vision-Language Models, PRISM overcomes the latency and domain fragility limitations of prior data-free methods. Our synergistic mechanisms—the Hybrid VLM Teacher for prototype refinement and Adaptive Router for statistical gating—ensure robust detection without compromising clean accuracy. Extensive evaluations confirm PRISM neutralizes state-of-the-art attacks, achieving negligible Attack Success Rates with superior efficiency. As a model-agnostic solution, PRISM secures deployed models against evolving threats, charting a new direction for multimodal intelligence in trusted AI.

## Impact Statements

This paper introduces a novel paradigm for securing machine learning systems against backdoor attacks through external semantic auditing. By enabling the detection of malicious triggers without accessing private training data or retraining, our work facilitates the safe deployment of third-party models in Model-as-a-Service (MaaS) environments. This capability is particularly critical for high-stakes domains, such as healthcare and autonomous driving, where ensuring the integrity of “black-box” models is paramount for public safety.

However, we acknowledge that our framework relies on the capabilities and robustness of pre-trained Vision-Language Models (VLMs). Consequently, any inherent biases or hallucinations present in these foundation models could potentially propagate to the auditing process. Furthermore, as demonstrated in our analysis of auditor-aware adaptive attacks (Section 5.5.2), the external auditor remains susceptible to input-level semantic manipulation—such as typographic triggers—which can partially bypass the semantic gatekeeper and raise the Attack Success Rate (e.g., to 15.6%). While our work focuses on defense, we encourage future research to investigate both the fairness of foundation models and their resilience against semantic adversarial examples to ensure equitable and robust security across diverse threat landscapes.

## References

Bai, S., Chen, K., Liu, X., Wang, J., Ge, W., Song, S., Dang, K., Wang, P., Wang, S., Tang, J., et al. Qwen2.5-vl technical report. *arXiv preprint arXiv:2502.13923*, 2025.

Barni, M., Kallas, K., and Tondi, B. A new backdoor attack in cnns by training set corruption without label poisoning. In *2019 IEEE International Conference on Image Processing (ICIP)*, pp. 101–105. IEEE, 2019.

Chen, X., Liu, C., Li, B., Lu, K., and Song, D. Targeted backdoor attacks on deep learning systems using data poisoning. *arXiv preprint arXiv:1712.05526*, 2017.

Chen, Y., Shao, S., Huang, E., Li, Y., Chen, P.-Y., Qin, Z., and Ren, K. REFINE: Inversion-free backdoor defense via model reprogramming. In *The Thirteenth International Conference on Learning Representations*, 2025. URL <https://openreview.net/forum?id=4IYdCws9fc>.

Gai, K., Wang, D., Yu, J., Zhu, L., and Wu, Q. A vision-language pre-training model-guided approach for mitigating backdoor attacks in federated learning. *arXiv preprint arXiv:2508.10315*, 2025.

Girdhar, R., El-Nouby, A., Liu, Z., Singh, M., Alwala, K. V., Joulin, A., and Misra, I. Imagebind: One embedding space to bind them all. In *Proceedings of the IEEE/CVF conference on computer vision and pattern recognition*, pp. 15180–15190, 2023.

Gu, T., Liu, K., Dolan-Gavitt, B., and Garg, S. Badnets: Evaluating backdooring attacks on deep neural networks. *IEEE Access*, 7:47230–47244, 2019.

Guo, J., Li, Y., Chen, X., Guo, H., Sun, L., and Liu, C. SCALE-UP: An efficient black-box input-level backdoor detection via analyzing scaled prediction consistency. In *The Eleventh International Conference on Learning Representations*, 2023. URL <https://openreview.net/forum?id=o0LFPcoFKnr>.

Ikezogwo, W., Seyfioglu, S., Ghezloo, F., Geva, D., Sheikh Mohammed, F., Anand, P. K., Krishna, R., and Shapiro, L. Quilt-1m: One million image-text pairs for histopathology. *Advances in neural information processing systems*, 36:37995–38017, 2023.

Jha, R., Hayase, J., and Oh, S. Label poisoning is all you need. *Advances in Neural Information Processing Systems*, 36, 2024.

Li, C., Pang, R., Xi, Z., Du, T., Ji, S., Yao, Y., and Wang, T. An embarrassingly simple backdoor attack on self-supervised learning. In *Proceedings of the IEEE/CVF International Conference on Computer Vision*, pp. 4367–4378, 2023.

Li, Y., Li, Y., Wu, B., Li, L., He, R., and Lyu, S. Invisible backdoor attack with sample-specific triggers. In *Proceedings of the IEEE/CVF international conference on computer vision*, pp. 16463–16472, 2021.

Liang, S., Zhu, M., Liu, A., Wu, B., Cao, X., and Chang, E.-C. Badclip: Dual-embedding guided backdoor attack on multimodal contrastive learning. In *Proceedings of the IEEE/CVF Conference on Computer Vision and Pattern Recognition*, pp. 24645–24654, 2024.

Lin, J., Xu, L., Liu, Y., and Zhang, X. Composite backdoor attack for deep neural network by mixing existing benign features. In *Proceedings of the 2020 ACM SIGSAC Conference on Computer and Communications Security*, pp. 113–131, 2020.

Liu, H., Li, C., Li, Y., and Lee, Y. J. Improved baselines with visual instruction tuning. In *Proceedings of the IEEE/CVF Conference on Computer Vision and Pattern Recognition*, pp. 26296–26306, 2024.

Liu, X., Li, M., Wang, H., Hu, S., Ye, D., Jin, H., Wu, L., and Xiao, C. Detecting backdoors during the inference stage based on corruption robustness consistency. In *Proceedings of the IEEE/CVF Conference on Computer Vision*

and Pattern Recognition (CVPR), pp. 16363–16372, June 2023.

Nguyen, T. A. and Tran, A. Input-aware dynamic backdoor attack. *Advances in Neural Information Processing Systems*, 33:3454–3464, 2020a.

Nguyen, T. A. and Tran, A. T. Wanet-imperceptible warping-based backdoor attack. In *International Conference on Learning Representations*, 2020b.

Pang, L., Sun, T., Ling, H., and Chen, C. Backdoor cleansing with unlabeled data. In *Proceedings of the IEEE/CVF Conference on Computer Vision and Pattern Recognition*, pp. 12218–12227, 2023.

Phan, H., Xiao, J., Sui, Y., Zhang, T., Tang, Z., Shi, C., Wang, Y., Chen, Y., and Yuan, B. Clean and compact: Efficient data-free backdoor defense with model compactness. In *European Conference on Computer Vision*, pp. 273–290. Springer, 2024.

Radford, A., Kim, J. W., Hallacy, C., Ramesh, A., Goh, G., Agarwal, S., Sastry, G., Askell, A., Mishkin, P., Clark, J., et al. Learning transferable visual models from natural language supervision. In *International conference on machine learning*, pp. 8748–8763. PMLR, 2021.

Shi, Y., Du, M., Wu, X., Guan, Z., Sun, J., and Liu, N. Black-box backdoor defense via zero-shot image purification. In *Thirty-seventh Conference on Neural Information Processing Systems*, 2023.

Sun, T., Pang, L., Chen, C., and Ling, H. Mask and restore: Blind backdoor defense at test time with masked autoencoder. *arXiv preprint arXiv:2303.15564*, 2023.

Team, G., Kamath, A., Ferret, J., Pathak, S., Vieillard, N., Merhej, R., Perrin, S., Matejovicova, T., Ramé, A., Rivière, M., et al. Gemma 3 technical report. *arXiv preprint arXiv:2503.19786*, 2025.

Turner, A., Tsipras, D., and Madry, A. Label-consistent backdoor attacks. *arXiv preprint arXiv:1912.02771*, 2019.

Wang, X., Zhu, Z., Jin, Z., Chen, H., and Lim, T. J. Rethinking lipschitzness data-free backdoor defense. In *Proceedings of the 34th ACM International Conference on Information and Knowledge Management*, pp. 3113–3122, 2025.

Wang, Z., Zhai, J., and Ma, S. Bppattack: Stealthy and efficient trojan attacks against deep neural networks via image quantization and contrastive adversarial learning. In *Proceedings of the IEEE/CVF Conference on Computer Vision and Pattern Recognition*, pp. 15074–15084, 2022.

Wu, B., Chen, H., Zhang, M., Zhu, Z., Wei, S., Yuan, D., and Shen, C. Backdoorbench: A comprehensive benchmark of backdoor learning. *Advances in Neural Information Processing Systems*, 35:10546–10559, 2022.

Wu, B., Chen, H., Zhang, M., Zhu, Z., Wei, S., Yuan, D., Zhu, M., Wang, R., Liu, L., and Shen, C. Backdoorbench: A comprehensive benchmark and analysis of backdoor learning, 2024. URL <https://arxiv.org/abs/2407.19845>.

Xu, B., Dai, X., Tang, D., and Zhang, K. One surrogate to fool them all: Universal, transferable, and targeted adversarial attacks with clip. In *Proceedings of the 2025 ACM SIGSAC Conference on Computer and Communications Security*, pp. 3087–3101, 2025a.

Xu, B., Yang, F., Dai, X., Tang, D., and Zhang, K. Clip-guided backdoor defense through entropy-based poisoned dataset separation. In *Proceedings of the 33rd ACM International Conference on Multimedia*, pp. 7415–7423, 2025b.

Xu, B., Yang, F., Tang, D., Dai, X., and Zhang, K. Breaking the stealth-potency trade-off in clean-image backdoors with generative trigger optimization. *arXiv preprint arXiv:2511.07210*, 2025c.

Yang, W., Gao, J., and Mirzasoleiman, B. Better safe than sorry: Pre-training CLIP against targeted data poisoning and backdoor attacks. In *Forty-first International Conference on Machine Learning*, 2024. URL <https://openreview.net/forum?id=ycLHJuLYuD>.

Zhai, X., Mustafa, B., Kolesnikov, A., and Beyer, L. Sigmoid loss for language image pre-training. In *Proceedings of the IEEE/CVF international conference on computer vision*, pp. 11975–11986, 2023.

Zheng, R., Tang, R., Li, J., and Liu, L. Data-free backdoor removal based on channel lipschitzness. In *European Conference on Computer Vision*, pp. 175–191. Springer, 2022.

## A. Theoretical Foundations of Adaptive Thresholding

In the methodology, we introduced an adaptive thresholding mechanism to handle the non-Gaussian distribution of the logit margin  $\Delta$ . While the Central Limit Theorem suggests that distributions approach normality asymptotically, the finite sample distributions of neural network logits—especially after the exponential transformation in Eq. (2)—often exhibit significant asymmetry (skewness). To address this, we employ the **Cornish-Fisher Expansion**, a moment-based approximation technique, rather than assuming a strict parametric distribution.

### A.1. Edgeworth and Cornish-Fisher Expansions

Let  $X$  be a random variable representing the logit margin  $\Delta$  for a specific class, characterized by its mean  $\mu$ , variance  $\sigma^2$ , and skewness  $\gamma$ . We define the standardized variable  $Z = (X - \mu)/\sigma$ . The *Edgeworth expansion* provides a refinement to the standard normal approximation by adding correction terms based on higher-order cumulants. The probability density function (PDF) of the standardized variable  $Z$  can be approximated as:

$$f_Z(z) \approx \phi(z) \left[ 1 + \frac{\gamma}{6} H_3(z) \right], \quad (4)$$

where  $\phi(z)$  is the standard normal PDF, and  $H_3(z) = z^3 - 3z$  is the third Hermite polynomial.

However, for outlier detection and thresholding, we are strictly interested in the *quantiles* of the distribution rather than the density. The *Cornish-Fisher expansion* inverts the Edgeworth expansion to express the quantile  $w_\alpha$  of the non-normal distribution  $Z$  in terms of the quantile  $z_\alpha$  of the standard normal distribution (where  $\Phi(z_\alpha) = \alpha$ ).

The first few terms of the Cornish-Fisher expansion for the  $p$ -th quantile are given by:

$$w_p \approx z_p + \frac{1}{6}(z_p^2 - 1)\gamma + O(n^{-1}), \quad (5)$$

where:

- $w_p$  is the approximate quantile of the standardized margin distribution.
- $z_p$  is the standard normal quantile (corresponding to our hyperparameter  $\zeta$ ).
- $\gamma$  is the skewness of the margin distribution.

### A.2. Derivation of the Threshold Formula

In PRISM, we seek a threshold  $\tau$  that separates benign samples (high consistency) from potential attacks (low consistency) with a confidence level determined by the base

Z-score  $\zeta$ . Mapping back from the standardized domain to the original domain  $X \sim \mathcal{D}(\mu, \sigma, \gamma)$ , the threshold  $\tau$  is derived as:

$$\begin{aligned} \tau &= \mu + w_p \cdot \sigma \\ &\approx \mu + \left[ \zeta + \frac{\gamma}{6}(\zeta^2 - 1) \right] \cdot \sigma. \end{aligned} \quad (6)$$

Let the skewness-adjusted coefficient be  $\tilde{\zeta} = \zeta + \frac{\gamma}{6}(\zeta^2 - 1)$ . This directly corresponds to the implementation in our Adaptive Router:

$$\tau_{adaptive} = \mu + \tilde{\zeta} \cdot \sigma. \quad (7)$$

**Applicability and Robustness.** This derivation demonstrates that our correction term is not a heuristic but a first-order statistical approximation that adjusts the acceptance region based on the asymmetry of the discrepancy distribution. For a distribution with a heavy left tail (negative skewness),  $\tilde{\zeta}$  decreases, effectively lowering the threshold to avoid rejecting valid benign samples. To ensure numerical stability during the online estimation process—where extreme outliers might temporarily distort moments—we strictly clamp the estimated skewness  $\gamma$  to the range  $[-10, 10]$ . This prevents the threshold from diverging due to finite-sample volatility.

## B. Online Estimation of Statistical Moments

PRISM employs a memory-efficient online mechanism to update the statistical moments (mean, variance, skewness) of the margin  $\Delta$  without storing historical data. This ensures  $O(1)$  time complexity and minimal memory footprint.

Let  $S_{1,n}$ ,  $S_{2,n}$ , and  $S_{3,n}$  denote the sums of the first, second, and third powers of the incoming data stream up to step  $n$ , respectively. For a new batch of samples  $\mathbf{x} = \{x_1, \dots, x_m\}$  at step  $t$ , we update the raw moments as follows:

$$N_t = N_{t-1} + m \quad (8)$$

$$S_{1,t} = S_{1,t-1} + \sum_{i=1}^m x_i \quad (9)$$

$$S_{2,t} = S_{2,t-1} + \sum_{i=1}^m x_i^2 \quad (10)$$

$$S_{3,t} = S_{3,t-1} + \sum_{i=1}^m x_i^3 \quad (11)$$

The expected values (raw moments) are estimated as:

$$E[X] = \frac{S_{1,t}}{N_t}, \quad E[X^2] = \frac{S_{2,t}}{N_t}, \quad E[X^3] = \frac{S_{3,t}}{N_t}. \quad (12)$$

To compute the Cornish-Fisher threshold, we require the **central moments**. These are derived algebraically from the raw moments:

1. **Mean** ( $\mu$ ):

$$\mu = E[X]$$

2. **Variance** ( $\sigma^2$ ):

$$\sigma^2 = E[X^2] - (E[X])^2$$

To prevent division-by-zero errors in stable environments where variance is near-zero, we apply a numerical floor:  $\sigma^2 = \max(\sigma^2, \epsilon)$  with  $\epsilon = 10^{-8}$ .

3. **Skewness** ( $\gamma$ ): The third central moment  $\mu_3 = E[(X - \mu)^3]$  is expanded as:

$$\begin{aligned} \mu_3 &= E[X^3 - 3X^2\mu + 3X\mu^2 - \mu^3] \\ &= E[X^3] - 3\mu E[X^2] + 2\mu^3 \end{aligned} \quad (13)$$

The Fisher-Pearson coefficient of skewness is then:

$$\gamma = \frac{\mu_3}{\sigma^3} = \frac{E[X^3] - 3\mu E[X^2] + 2\mu^3}{(E[X^2] - \mu^2)^{3/2}}$$

## C. Prototype Refinement and Hybrid Fusion

This section details the update rules for the Hybrid VLM Teacher, specifically the explicit formulation for prototype updates and the handling of generative VLM embeddings.

### C.1. Online Prototype Update Rule

To bridge the domain gap, we dynamically refine the visual prototypes (class centroids)  $\mathcal{C} = \{c_1, \dots, c_K\}$ . Let  $c_k^{(t)}$  be the prototype for class  $k$  at step  $t$ , and  $N_k^{(t)}$  be the cumulative count of *verified clean* samples assigned to class  $k$ .

Upon receiving a batch of test samples, we first filter them using the current Adaptive Router. Only samples satisfying  $\Delta > \tau$  are used for updates. For a batch of certified clean samples  $\mathcal{B}_{clean}$  belonging to class  $k$ , the prototype is updated via Cumulative Moving Average (CMA) to ensure statistical inertia:

$$c_k^{(t)} = \text{Normalize} \left( \frac{N_k^{(t-1)} c_k^{(t-1)} + \sum_{x \in \mathcal{B}_{clean}^k} z_{img}(x)}{N_k^{(t-1)} + |\mathcal{B}_{clean}^k|} \right), \quad (14)$$

where  $z_{img}(x)$  is the normalized visual embedding of the input. The  $\text{Normalize}(\cdot)$  operation projects the vector back onto the unit hypersphere ( $\|c\|_2 = 1$ ), ensuring compatibility with cosine similarity metrics. This explicit update allows the VLM to gradually adapt its visual expectation from generic pre-training features to the specific distribution of the test stream.

### C.2. Hybrid Fusion Strategy

The VLM logit  $S_{VLM}$  is computed as a weighted fusion:

$$S_{VLM} = \lambda \cdot S_{text} + (1 - \lambda) \cdot S_{proto} \quad (15)$$

To ensure score compatibility between the two streams:

- **Embedding Models (CLIP/SigLIP):** Both  $S_{text}$  and  $S_{proto}$  represent cosine similarities, naturally bounded in  $[-1, 1]$ .
- **Generative Models (Qwen/LLaVA):** For  $S_{text}$ , we calculate the log-likelihood of the class name tokens. For  $S_{proto}$ , we extract the visual features  $z_{img}$  directly from the underlying Vision Encoder (e.g., the ViT component before the LLM projector). This allows us to maintain a visual prototype space even for generative models. The text scores are min-max normalized within the batch to match the scale of cosine similarity before fusion.

## D. Experimental Setting Details

### D.1. Warm-up and Initialization Strategy

A critical challenge in online statistical defense is the "cold start" problem, where moment estimates (especially skewness) are unstable due to insufficient sample size. We implement a robust warm-up strategy:

1. **Confidence Weighting:** We define a confidence coefficient  $\alpha_t = \min(1.0, \frac{N_t}{N_{warmup}})$ , where  $N_{warmup} \approx 100$ .
2. **Correction Dampening:** During the warm-up phase, the skewness correction term in the Cornish-Fisher expansion is dampened by  $\alpha_t$ . The effective threshold becomes:

$$\tau_{eff} = \mu + \left[ \zeta + \alpha_t \cdot \frac{\gamma}{6} (\zeta^2 - 1) \right] \cdot \sigma \quad (16)$$

When  $N_t$  is small ( $\alpha_t \rightarrow 0$ ), the threshold reverts to a conservative Gaussian estimate ( $\tau = \mu + \zeta\sigma$ ), preventing erratic behavior from noisy skewness estimates. As  $N_t$  grows, the system smoothly transitions to full skewness-aware adaptive thresholding.

### D.2. Vision-Language Model Configuration

**Discriminative Backbones.** We utilize official pre-trained weights from OpenCLIP. Specifically, we employ ViT-B-32 pre-trained on LAION-2B for CLIP and ViT-B-16 for SigLIP. Embeddings are normalized to the hypersphere.

**Generative Backbones.** For models like Qwen2.5-VL and LLaVA-1.5, we utilize a Key-Value (KV) cache strategy

Table 5. Evaluation of ML Trust Chain on Medical Dataset (LC25000). The Trust Chain strategy effectively bridges the gap between the low-accuracy trusted anchor (CLIP) and the high-accuracy untrusted expert (QuiltNet).

Scenario	Configuration / Pipeline	Role	CA (%)	ASR (%)
Baselines	Trusted Universal VLM (CLIP)	Auditor	53.7	0.6
	Untrusted Domain VLM (QuiltNet)	Auditor	75.2	98.1
	Poisoned Victim Model	Victim	<b>98.7</b>	98.3
Direct Auditing	CLIP $\xrightarrow{\text{audit}}$ Victim	Defense	87.9	<b>3.5</b>
	Poisoned QuiltNet $\xrightarrow{\text{audit}}$ Victim	Defense	96.4	98.4 (Fail)
Trust Chain (Ours)	Step 1: CLIP $\xrightarrow{\text{audit}}$ QuiltNet	Intermediate	79.2	3.2
	Step 2: Sanitized QuiltNet $\xrightarrow{\text{audit}}$ Victim	Final Defense	<b>95.8</b>	<b>4.5</b>

to optimize inference. We employ a hierarchical filtering strategy where a lightweight CLIP model first selects the Top- $K$  (default  $K = 100$ ) candidates, which are then re-ranked by the Generative VLM using the prompt: “*Please answer with exactly one label from the list above.*”

### D.3. PRISM Hyperparameters

**Hybrid Fusion Weight ( $\lambda$ ).** We set  $\lambda = 0.5$  by default (denoted as `text_anchor_weight`), balancing pre-trained semantic knowledge with online visual adaptation.

**Adaptive Thresholding.** We use a base Z-score coefficient  $\zeta = -2.0$ , corresponding to the lower 2.5% quantile of a normal distribution.

### D.4. Prompt Engineering

We maximize reproducibility by using standardized templates without extensive engineering. For numeric datasets (e.g., SVHN), class labels are mapped to natural language (e.g., “1”  $\rightarrow$  “the digit one”).

Table 6. Representative prompt templates used for VLM zero-shot anchors.

Dataset	Template Structure
CIFAR-10/100	“a photo of a {label}.”
GTSRB	“a close up photo of a ‘{label}’ traffic sign.”
Food101	“a photo of {label}, a type of food.”
DTD	“a photo of a {label} texture.”
Medical	“a histopathology image of {label}.”

## E. Case Study: ML Trust Chain

We investigate a “worst-case” scenario where the auditor itself is backdoored. We use the LC25000 histopathological dataset. We assume a **Collusive Threat Model** where both the Victim Model (ResNet) and the Specialized Auditor (QuiltNet) are poisoned with the same trigger.

**The Trust Chain Solution.** We construct a hierarchical pipeline: Trusted Weak Generalist (CLIP)  $\rightarrow$  Untrusted Strong Specialist (QuiltNet)  $\rightarrow$  Victim. First, the weak but clean Generalist (CLIP) audits the Untrusted Specialist. Although CLIP has low classification accuracy (53.7%), it

effectively detects the distributional anomaly of the trigger, sanitizing the input stream for QuiltNet. The sanitized QuiltNet then audits the Victim. Results in Table 5 show this method recovers Clean Accuracy to 95.8% while suppressing ASR to 4.5%.

## F. Case Study: Building an ML Trust Chain in Specialized Domains with a Backdoored Auditor

While PRISM demonstrates strong performance with trusted general-purpose VLMs, a practical dilemma arises in specialized domains like healthcare. General VLMs (e.g., CLIP) often lack the necessary domain expertise, while specialized VLMs (e.g., QuiltNet (Ikezogwo et al., 2023)) are typically third-party assets that may themselves be untrusted. In this section, we investigate a “worst-case” scenario where the auditor itself is backdoored. We propose a *Machine Learning Trust Chain* paradigm to secure the inference pipeline, using the LC25000 histopathological dataset as a testbed.

**Collusive Threat Model.** We assume a stringent threat environment involving two compromised models. First, the **Victim Model** (ResNet) is embedded with a standard backdoor. Second, the **Specialized Auditor (QuiltNet) is also poisoned**. Crucially, to maximize the difficulty of detection, we employ a *Collusive Threat Model*: we use the BadCLIP (Liang et al., 2024) framework to inject the **exact same trigger** into the QuiltNet auditor as used in the victim model. This creates a scenario where both the victim and the auditor are aligned to misclassify the trigger, theoretically bypassing standard consistency checks. The only “Root of Trust” is a standard, off-the-shelf **Generalist VLM** (CLIP), which is assumed to be clean but possesses poor zero-shot accuracy ( $\sim 53\%$ ) on this specialized medical task.

**The Dilemma of Direct Auditing.** Directly deploying either VLM as a standalone auditor fails to balance security and utility. If we employ the trusted Generalist (CLIP) to audit the victim directly, it successfully suppresses the Attack Success Rate (ASR) to 3.5% due to its statistical

independence from the trigger. However, its lack of domain knowledge leads to a catastrophic drop in Clean Accuracy (CA) from 98.7% to 87.9%, deeming it unusable for medical diagnosis. Conversely, utilizing the Specialized Auditor (QuiltNet) maintains high clean accuracy (96.4%) but fails completely as a defense mechanism. Because QuiltNet contains the same backdoor as the victim, it "colludes" with the victim's prediction on poisoned samples, resulting in an ASR of 98.4%.

**Establishing the Trust Chain.** To resolve this, we construct a hierarchical auditing pipeline: *Trusted Weak Generalist*  $\rightarrow$  *Untrusted Strong Specialist*  $\rightarrow$  *Victim*. The process operates in two stages. First, the weak but clean Generalist (CLIP) audits the input stream of the Untrusted Specialist (QuiltNet). Although CLIP cannot classify the medical images accurately, it is highly effective at detecting the distributional anomaly of the trigger pattern via our statistical margin test, effectively "sanitizing" the QuiltNet inference stream. Second, this dynamically sanitized QuiltNet is used to audit the final Victim Model.

**Results and Implications.** This hierarchical strategy effectively decouples the defense capability from the auditor's own integrity regarding the trigger. By filtering the specialized auditor's inputs using a generalist root of trust, we recover the system's security. The Trust Chain suppresses the ASR to 4.5%—comparable to using the clean CLIP directly—while achieving a final Clean Accuracy of 95.8%, significantly outperforming the naive generalist approach. This result confirms that PRISM can defend against a compromised victim model even when the domain-specific auditor contains the same backdoor, provided a clean (even if weak) foundation model is available to initiate the chain of trust.

## G. Empirical Validation of the Moment-Based Distribution Approximation

The core mechanism of PRISM's Adaptive Router relies on the observation that the logit margin  $\Delta$ —defined as the exponential difference between the VLM's support for the victim's prediction and the next best class—**exhibits significant asymmetry**. This distributional characteristic necessitates the use of the Cornish-Fisher expansion to calibrate thresholds, rather than relying on standard Gaussian statistics which assume symmetry. To validate this, we visualize empirical distributions of  $\Delta$  across diverse conditions.

The visualizations reveal that the distribution of benign samples (highlighted in blue) consistently deviates from normality. In the upper panel (Figure 8), which details the distribution under BadNets attacks across five distinct datasets, we observe that the distribution shape varies significantly by domain. For instance, simpler datasets like

MNIST exhibit sharper peaks with heavy tails, whereas complex domains like ImageNet show broader variance. A standard normal approximation would fail to capture these tail behaviors, leading to either high false rejection rates or missed detections.

However, the **approximated density curves** (shown in yellow), derived via the **Edgeworth expansion** using the online estimates of the first three moments, demonstrate a tight alignment with the empirical histograms. This confirms that incorporating skewness  $\gamma$  into the threshold calculation allows the decision boundary (red dashed line) to dynamically adapt to the natural asymmetry of the semantic margin without enforcing a strict parametric assumption.

Furthermore, the lower panel (Figure 10) demonstrates the robustness of this approximation across 12 different attack modalities on CIFAR-10. Despite the variation in attack strategies—ranging from patch-based BadNets to clean-image FLIP attacks—the benign distributions remain consistent, and the moment-based fitted curves accurately encapsulate the safe acceptance regions. Notably, the backdoored samples (highlighted in red) and misclassified inputs (highlighted in orange) predominantly fall into the lower-margin regions below the adaptive threshold. The separation illustrates that while the benign data manifold is complex and asymmetric, it is statistically distinct from the backdoor distribution, and our moment-based method provides a mathematically grounded approach to isolate it efficiently.

## H. Details of Adaptive Auditor-Aware Attack

To rigorously evaluate the robustness of PRISM under a strong adaptive threat model—where the adversary specifically targets the "trusted" VLM auditor—we design a *Semantic Typography Attack*. Unlike standard backdoor triggers that rely on abstract patterns, this attack embeds semantic text information into the image to mislead the VLM's zero-shot prediction.

**Implementation Details.** We conduct this experiment on the CIFAR-10 dataset targeting the "Airplane" class (Class 0). The attack inserts the text string "Plane" into the benign images. The text is rendered in a bright red color (RGB: 255, 0, 0). To minimize the occlusion of the original object's visual features, the text is placed in the **bottom-left corner** of the image with a 1-pixel margin. The text height is controlled to be approximately 21% of the image height.

Visualizations of the attack samples are provided in Figure 9. As observed, the red text trigger is distinct yet leaves the main body of the original object (e.g., the cat) visible, creating a scenario where the victim model (activated by the trigger) and the visual perception of the VLM (observing the object) may conflict.

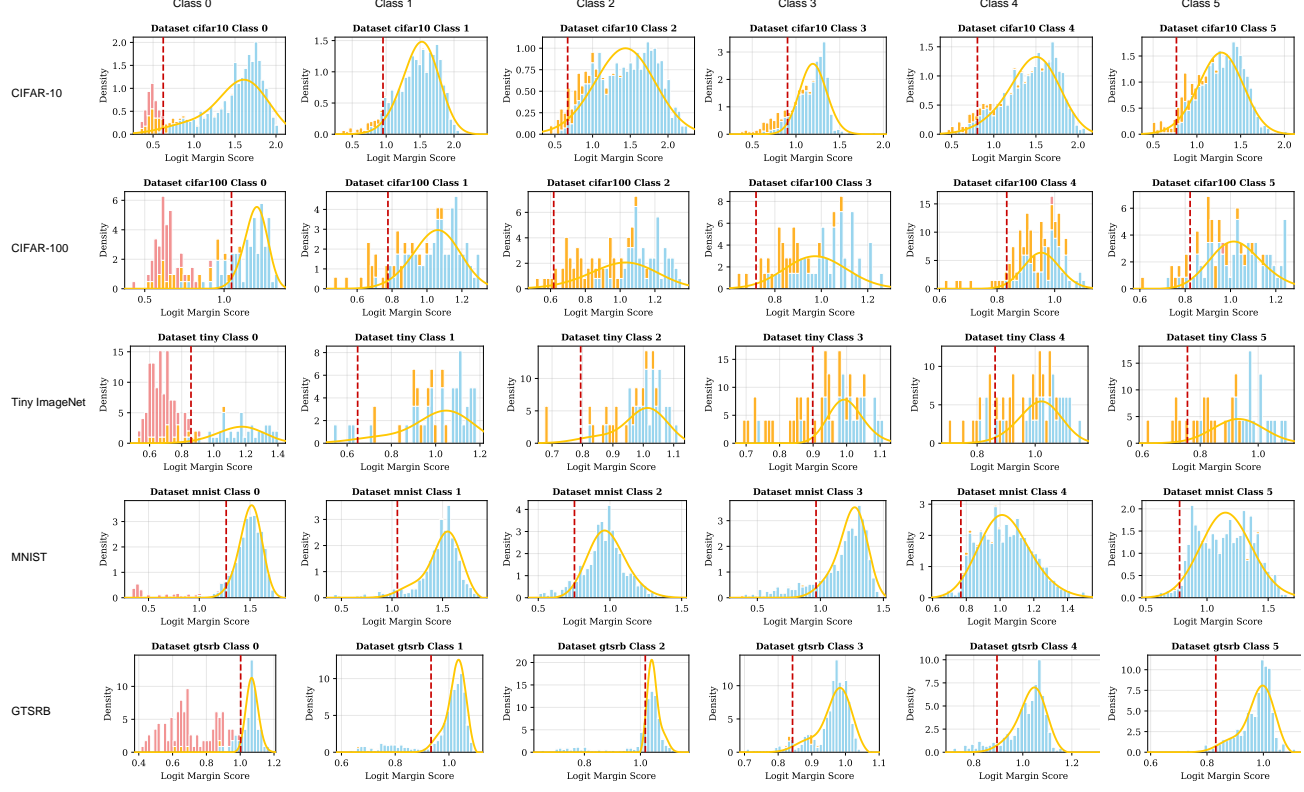


**Figure 8. Distribution of Logit Margin across different datasets (BadNets).** The histograms visualize the density of the logit margin  $\Delta$ . Benign samples are highlighted in blue, successful backdoor samples in red, and misclassified samples in orange. The yellow curve represents the **density approximation derived via Edgeworth expansion** using online moment estimates. The vertical red dashed line indicates the adaptive threshold  $\tau$ . The tight alignment validates that our skewness-aware modeling effectively distinguishes high-consistency benign samples from low-consistency attacks.



**Figure 9. Visualization of Adaptive Text Prompt Attack Samples.** The text “Plane” is superimposed on the bottom-left corner of the images (e.g., a Frog or a Cat) to act as a semantic trigger targeting the VLM auditor.

## I. Defense against Feature Mixing Backdoors

To comprehensively evaluate the robustness of PRISM, we further consider the *Feature Mixing Backdoor* (FMB) attacks (Lin et al., 2020). Unlike standard patch-based attacks, FMB is designed to confuse VLM semantics by linearly blending features from multiple classes (e.g., mixing the pixel values of a source image with another image). We evaluate our defense against both the one-to-one (o2o) and all-to-one (a2o) attack variants.

The results are presented in Table 8. PRISM exhibits strong defense performance, suppressing the Attack Success Rate (ASR) to  $\leq 2.2\%$  in both settings while maintaining or even slightly improving Clean Accuracy (CA).

**Analysis.** The effectiveness of PRISM against FMB can be attributed to the semantic inconsistency it introduces. While feature mixing may successfully confuse the VLM between the two mixed *source* classes (e.g., the VLM might hesitate between “Cat” and “Dog”), the resulting image does not semantically resemble the malicious *target* label (e.g., “Airplane”). Since the victim model is forced to predict the target label with high confidence, while the VLM finds no semantic evidence for that target, the logit margin used by PRISM remains high. This allows our adaptive router to correctly flag these inputs as anomalous distributions.

## J. Performance Comparison on Domain-Specific Datasets

Table 7 presents a detailed comparison on the GTSRB dataset under a stealthy 1% poison rate. This scenario is particularly challenging for existing defenses: model repairing methods like CLP and C&C often damage the Clean Accuracy (CA) significantly due to the domain gap, while input robustness methods fail to detect the sparse trigger samples. As shown by the extensive red highlights, all baseline meth-

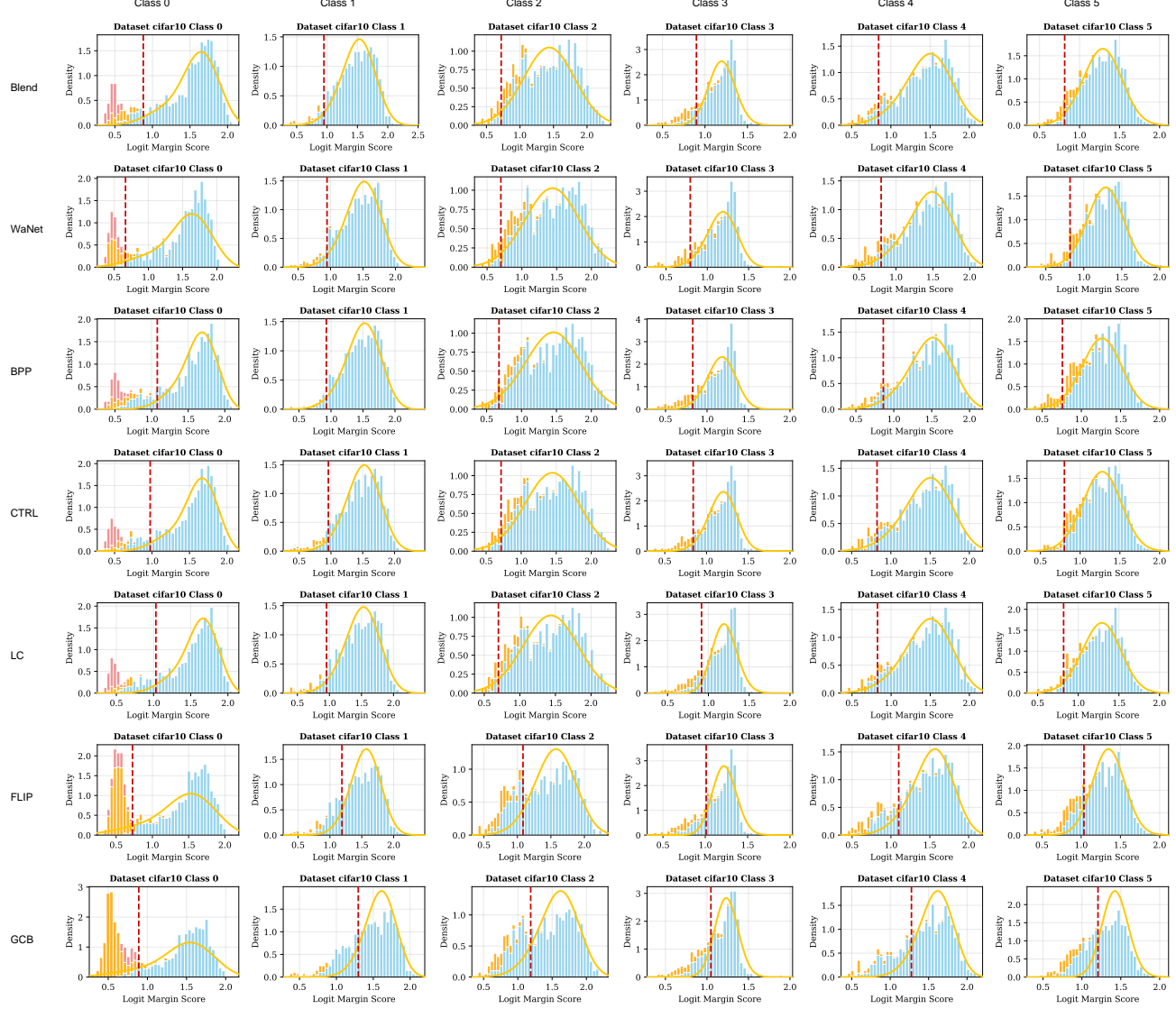


**Figure 10. Distribution of Logit Margin across different attack types (CIFAR-10).** This visualization validates the robustness of our **moment-based approximation** against 12 diverse backdoor attacks, including dynamic and clean-label variants. Despite the diversity in attack vectors, the benign distributions maintain characteristic asymmetries that are accurately captured by our adaptive thresholding logic.

ods fail to simultaneously maintain high CA and low ASR. In contrast, PRISM successfully suppresses the average ASR to 3.6% while maintaining a high CA of 93.4%, outperforming the best baseline by a significant margin. This underscores PRISM’s superiority in specialized domains where pre-trained knowledge must be carefully adapted.

## K. Defense Independence from Zero-Shot Performance

A common concern is whether VLM-based defenses rely heavily on the VLM’s inherent zero-shot classification accuracy. Table 9 addresses this by evaluating PRISM across representative datasets with varying levels of zero-shot performance, ranging from 62.3% (CIFAR-100) down to 25.1%

(GTSRB). To rigorously quantify detection efficacy, we adopt a utility-centric metric formulation: **True Positive Rate (TPR)** is calculated strictly over *effective* attacks (backdoor samples that successfully fool the victim model into the target class), while **False Positive Rate (FPR)** is computed solely on *correctly classified* clean samples. This unique calculation excludes ineffective attacks and already-misclassified clean inputs, preventing them from artificially inflating detection performance. Remarkably, even on GTSRB where the VLM’s raw accuracy is nearly random, PRISM effectively utilizes *relative* semantic inconsistency to distinguish attacks, achieving a high average TPR of 96.3% while maintaining a low FPR of 6.8%. The results confirm that our framework successfully recovers the victim model’s high utility (raising CA from the VLM’s 25.1% to

Table 7. Evaluation of test-time backdoor defenses on GTSRB (1% poison rate). ASRs below 15% are highlighted in **blue** to indicate a successful defense, while ASRs above 15% are denoted in **red** as failed defenses.

Defense →	Existing Backdoor Defenses														Naive VLM Baselines				PRISM (Ours)						
	No Defense		CLP		ScaleUp		BDMAE		ZIP		TeCo		C&C		LPP		Refine		Zero-shot		Ensemble				
	Attack ↓	CA	ASR	CA	ASR	CA	ASR	CA	ASR	CA	ASR	CA	ASR	CA	ASR	CA	ASR	CA	ASR	CA	ASR				
Classic	BadNet	98.5	91.4	97.1	16.7	92.6	0.1	97.7	5.1	98.6	1.5	98.5	91.3	88.0	5.1	96.8	0.4	97.9	0.1	25.1	0.3	91.7	45.2	95.6	0.0
	Blend	98.4	93.4	95.1	16.1	98.3	43.9	97.4	42.6	97.2	9.9	98.4	93.4	86.8	23.0	98.4	42.4	98.3	0.1	25.1	0.1	90.3	26.0	93.6	2.5
Dynamic	WaNet	98.6	70.7	89.8	47.8	97.5	31.1	96.4	25.5	93.4	49.3	98.6	70.4	95.4	49.5	93.5	11.3	97.4	1.3	25.1	0.2	92.4	16.0	93.0	0.8
	BPP	98.4	75.3	97.6	0.2	98.3	35.2	97.7	38.1	97.5	7.4	98.8	75.2	95.3	2.0	98.2	0.0	97.7	0.1	25.1	0.0	96.2	29.5	95.7	0.0
	IAB	98.3	67.3	94.8	1.2	98.4	39.9	97.1	17.5	97.4	12.7	93.0	31.3	88.9	15.2	97.3	3.4	98.4	0.0	25.1	0.1	91.9	5.1	95.7	0.0
	SSBA	98.3	95.8	94.8	62.8	98.3	92.0	97.3	86.9	96.6	64.5	91.9	6.9	79.5	88.6	94.5	68.5	98.3	0.8	25.1	0.1	91.1	45.1	90.9	7.6
Clean	CTRL	98.4	79.5	95.2	6.0	98.3	73.4	98.3	36.7	96.8	0.2	93.1	14.7	60.0	1.5	93.2	0.0	98.3	0.2	25.1	0.0	89.9	39.3	92.7	6.7
	SIG	98.4	78.2	87.9	45.7	98.4	41.9	97.2	46.0	97.1	43.5	98.4	67.8	78.2	16.9	97.8	40.4	98.1	0.5	25.1	0.0	90.3	31.6	92.7	0.8
	LC	98.4	80.5	95.2	1.5	98.4	69.9	97.6	3.8	97.1	0.1	93.4	21.7	86.5	0.6	98.3	1.0	98.3	0.0	25.1	0.2	90.8	31.0	93.0	9.9
Image	FLIP	95.6	38.8	86.3	0.7	94.5	3.4	91.2	4.6	91.0	3.5	95.6	38.7	64.4	9.5	95.0	2.2	94.6	25.1	25.1	0.0	88.2	0.9	92.2	4.8
	GCB	97.3	98.6	94.8	90.9	97.2	84.3	96.4	87.2	96.0	84.8	87.7	14.3	77.1	98.8	89.3	55.1	96.9	93.0	25.1	0.5	90.9	46.9	91.9	6.7
Average		98.0	79.0	93.5	26.3	97.3	46.8	96.8	35.8	96.2	25.2	95.2	47.8	81.8	28.2	95.7	20.4	97.7	11.0	25.1	0.1	91.2	28.8	93.4	3.6
CA Drop (smaller is better)		▼4.5		▼0.7		▼1.3		▼1.8		▼2.8		▼16.2		▼2.4		▼0.4		▼72.9		▼6.8		▼4.7			
ASR Drop (larger is better)		▼52.7		▼32.2		▼43.2		▼53.8		▼31.3		▼50.8		▼58.6		▼68.0		▼78.9		▼50.3		▼75.4			

Table 8. Defense performance against Feature Mixing Backdoors (FMB). We report Clean Accuracy (CA) and Attack Success Rate (ASR) percentages.

FMB Variant	No Defense		PRISM	
	CA	ASR	CA	ASR
One-to-One	92.0	85.0	93.4	0.0
All-to-One	91.5	77.7	92.9	2.2

93.4%) while consistently suppressing ASR, validating that PRISM operates as a robust semantic auditor rather than a simple classifier substitute.

## L. Robustness to Varying Poison Rates

Table 10 examines the sensitivity of PRISM to the adversary’s injection capability, testing poison rates of 1%, 5%, and 10% on both CIFAR-10 and GTSRB. Statistical defenses often struggle at extremes: low poison rates yield insufficient samples for estimation, while high rates can dominate the clean distribution. PRISM demonstrates consistent robustness across this spectrum. Even at a 10% poison rate on GTSRB, where the attack distribution is strong, PRISM maintains an ASR of 4.0% with negligible impact on clean accuracy. This stability is attributed to our online warm-up and selective update mechanism, which prevents the statistical moments from being skewed by the poisoned samples.

## M. Scalability Across 17 Datasets and VLM Architectures

To demonstrate the universality of our framework, Table 11 provides an extensive evaluation across 17 diverse datasets, comparing the standard CLIP backbone with the generative Qwen2.5-VL-7b. The results confirm that PRISM generalizes well to datasets with extreme class imbalances (e.g.,

Caltech101, IR=86.5) and varying granularities (e.g., ImageNet, 1000 classes). Notably, the generative Qwen2.5-VL-7b backbone achieves comparable or superior performance to CLIP, particularly in fine-grained tasks like StanfordCars and Food101. This indicates that PRISM is model-agnostic and can benefit from the continuous advancements in Large Vision-Language Models.

## N. Component Contribution Analysis

Table 12 offers a granular ablation study dissecting the contribution of Online Update, Prototype Refinement, and Skewness Correction. The contrast between CIFAR-100 (general domain) and GTSRB (specialized domain) is revealing.

- **Necessity of Online Update:** On GTSRB, removing the online update mechanism leads to a catastrophic failure (ASR surges to 23.7%), as the static VLM anchors fail to align with the traffic sign distribution.
- **Impact of Prototype Refinement:** Without visual prototypes, the Clean Accuracy drops significantly (e.g., -13.6% on GTSRB), highlighting their role in bridging the domain gap.
- **Role of Skewness Correction:** Removing skewness correction destabilizes the thresholding, causing increased false acceptances of attacks (higher ASR) or false rejections of clean data (lower CA).

These results confirm that all three components are essential for a robust, domain-adaptive defense.

Table 9. Results of PRISM on five representative datasets. The table includes Clean Accuracy (CA), Attack Success Rate (ASR), True Positive Rate (TPR), and False Positive Rate (FPR). PRISM defends against all 11 attacks across all datasets.

Dataset→	CIFAR10 (86.7%)				CIFAR100 (62.3%)				Tiny (57.8%)				MNIST (43.6%)				GTSRB (25.1%)							
	Attack↓	CA	ASR	TPR	FPR	CA	ASR	TPR	FPR	CA	ASR	TPR	FPR	CA	ASR	TPR	FPR	CA	ASR	TPR	FPR			
BadNet	93.9	0.0	98.9	3.4	71.5	▲1.3	0.0	100.0	9.3	62.9	▲6.4	0.0	99.0	12.5	99.4	▼0.1	7.8	98.9	5.5	95.6	▼2.8	0.0	99.0	2.9
Blend	94.2	0.0	100.0	4.7	72.4	▲1.5	0.0	100.0	9.8	58.7	▲1.9	0.0	99.0	9.8	99.3	▼0.1	6.7	100.0	5.5	93.6	▼4.9	2.5	95.7	4.9
WaNet	93.6	0.0	98.8	3.2	67.4	▲3.7	0.0	100.0	10.6	57.5	▲1.5	3.0	95.0	8.2	93.7	▼5.1	7.4	93.3	4.9	93.0	▼5.6	0.8	93.9	12.3
BPP	93.7	1.1	100.0	3.0	69.5	▲4.7	0.0	100.0	11.3	56.9	▼0.9	0.0	96.3	9.0	99.3	▼0.1	3.3	95.0	5.5	95.7	▼0.7	0.0	100.0	1.9
IAB	92.4	0.0	100.0	4.2	69.8	▲4.8	0.0	100.0	10.0	57.8	▲1.9	0.0	98.8	11.2	93.1	▼3.9	8.4	95.6	4.9	95.7	▼2.6	0.0	100.0	3.2
SSBA	93.8	0.0	98.8	4.1	72.2	▲2.0	0.0	97.8	8.5	62.7	▲6.0	0.0	100.0	19.1	94.5	▼2.4	2.4	95.1	3.2	90.9	▼7.4	7.6	93.8	10.7
CTRL	94.2	0.0	100.0	3.1	72.3	▲2.0	0.0	100.0	11.2	55.1	▼1.9	0.0	100.0	10.7	99.4	▼0.3	0.0	10.0	0.1	92.7	▼5.9	6.7	91.9	6.8
SIG	92.6	2.2	98.8	4.5	72.0	▲1.8	0.0	100.0	6.6	62.3	▲5.8	0.0	100.0	10.3	99.2	▼0.1	0.0	100.0	0.1	92.7	▼5.6	0.8	98.1	6.0
LC	94.6	0.0	100.0	2.2	73.2	▲1.9	0.0	100.0	9.4	62.5	▲6.3	0.0	100.0	11.6	99.2	▼0.1	0.0	100.0	0.0	93.0	▼5.4	9.9	94.0	12.1
FLIP	91.7	1.1	100.0	12.2	70.0	▼0.1	1.0	100.0	11.7	56.4	▼0.1	0.0	92.7	9.6	96.2	▼1.1	6.7	97.4	1.2	92.2	▼3.4	4.8	100.0	0.4
GCB	90.1	4.4	99.1	19.6	68.1	▼2.1	2.2	92.6	21.1	62.4	▲5.5	2.0	97.5	39.3	94.7	▼1.3	3.3	90.5	10.0	91.9	▼5.3	6.7	92.7	13.2
Average	93.2	0.8	99.5	5.8	70.8	▲2.0	0.3	99.1	10.9	59.9	▲3.3	0.5	98.0	13.8	97.3	▼1.2	4.4	88.7	3.7	93.4	▼4.5	3.6	96.3	6.8

Table 10. PRISM under poison rate of 1%, 5%, 10%. Results are shown with change values on the right side. PRISM can succeed under all poison rates and all datasets.

Dataset→	CIFAR10								GTSRB															
	Poison Rate→		1%		5%		10%		1%		5%		10%											
			CA	ASR	CA	ASR	CA	ASR			CA	ASR	CA	ASR	CA	ASR								
BadNets	94.4	▲1.2	0.0	▼73.8	93.9	▲1.6	0.0	▼87.9	94.0	▲2.2	0.0	▼93.8	95.6	▼2.8	0.0	▼91.4	96.5	▼0.8	0.8	▼92.7	96.2	▲0.2	0.5	▼94.1
Blend	94.5	▲0.7	0.0	▼94.1	94.2	▲0.7	0.0	▼99.4	94.0	▲0.3	0.0	▼99.8	93.6	▼4.9	2.5	▼97.4	95.9	▼2.7	0.8	▼99.1	95.1	▼1.8	1.0	▼99.0
WaNet	93.7	▲2.5	0.0	▼72.0	93.6	▲2.5	0.0	▼94.1	93.3	▲2.7	0.0	▼96.9	93.0	▼5.6	0.8	▼69.9	92.1	▼3.6	9.2	▼89.5	91.5	▼2.6	12.0	▼85.6
BPP	93.4	▲2.0	1.1	▼98.1	93.7	▲2.1	1.1	▼98.3	93.4	▲2.0	1.1	▼98.1	95.7	▼0.7	0.0	▼99.8	93.7	▼2.7	0.0	▼99.8	93.3	▼3.9	0.0	▼98.8
IAB	93.1	▲2.6	0.0	▼54.6	92.4	▲1.0	0.0	▼95.0	92.8	▲3.1	0.0	▼94.9	95.7	▼2.6	0.0	▼67.3	94.4	▼3.1	0.0	▼83.2	93.5	▼3.7	0.0	▼92.4
SSBA	94.0	▲0.6	0.0	▼99.7	93.8	▲0.8	0.0	▼97.3	94.1	▲1.2	0.0	▼97.3	90.9	▼7.4	7.6	▼88.2	96.8	▼1.4	0.0	▼99.3	96.6	▲0.2	0.5	▼98.5
CTRL	94.7	▲0.7	0.0	▼55.3	94.2	▲0.6	0.0	▼95.9	94.2	▲0.6	0.0	▼95.9	92.7	▼5.9	6.7	▼88.6	91.0	▼7.6	7.6	▼87.7	90.5	▼5.7	8.5	▼90.4
SIG	92.6	▼1.1	3.3	▼77.0	92.6	▼1.0	2.2	▼91.6	92.4	▼7.8	1.7	▼96.3	92.7	▼5.6	0.8	▼77.3	91.7	▼6.5	1.7	▼88.8	91.8	▼4.3	2.0	▼93.9
LC	94.5	▲1.0	0.0	▼68.3	94.6	▲1.1	0.0	▼98.4	93.7	▲9.3	1.1	▼98.7	93.0	▼5.4	9.9	▼70.6	92.1	▼6.3	10.9	▼59.9	91.5	▼5.1	11.5	▼78.8
FLIP	93.9	▲0.6	0.0	▼98.1	91.7	▲1.9	1.1	▼98.1	92.6	▲7.2	2.2	▼97.5	92.2	▼3.4	4.8	▼34.0	91.9	▼1.8	2.0	▼54.4	91.4	▼0.7	2.5	▼81.2
GCB	92.5	▲0.0	3.3	▼96.7	90.1	▲1.6	4.4	▼95.6	90.0	▲5.8	5.6	▼94.4	91.9	▼5.3	6.7	▼92.0	88.8	▼6.5	5.0	▼94.9	87.7	▼5.8	6.0	▼94.0
Average	93.8	▲1.0	0.7	▼80.7	93.2	▲1.2	0.8	▼95.6	93.1	▲3.8	1.1	▼96.7	93.4	▼4.5	3.6	▼79.7	93.2	▼3.9	3.5	▼86.3	92.6	▼3.0	4.0	▼91.5

Table 11. Expanded scalability defense results comparing CLIP and Qwen2.5-VL-7b under poison rate of 5%. ASRs below 20% are highlighted in blue (success), while ASRs above 20% are denoted in red (fail). **Qwen2.5-VL-7b** demonstrates robust defense performance comparable to or better than CLIP across most datasets.

Dataset	IR	Entropy	# Class	Size	RN50	CLIP						Qwen2.5-VL-7b									
						VLM		Blend		BPP		CTRL		VLM		Blend		BPP		CTRL	
						ΔCA	ASR	ΔCA	ASR	ΔCA	ASR	ΔCA	ASR	ΔCA	ASR	ΔCA	ASR	ΔCA	ASR		
SVHN	3.20	0.965	10	234M	95.5	13.4	▼1.6	0.8	▼1.9	1.6	▼1.8	1.8	64.5	▼4.8	3.6	▼4.6	6.5	▼4.5	8.0		
Country211	1.00	1.00	211	20.9G	6.8	17.2	▲5.3	0.0	▲5.4	1.4	▲5.3	0.0	21.7	▲10.1	0.0	▲10.2	0.0	▲10.6	0.0		
GTSRB	12.5	0.920	43	689M	97.8	32.6	▼4.9	2.5	▼0.7	0.0	▼5.9	6.7	52.5	▼4.8	0.8	▼5.9	6.4	▼4.7	0.8		
FER2013	16.0	0.932	7	950M	63.0	41.4	▼5.6	0.0	▼3.8	4.8	▼4.7	4.8	27.6	▼4.4	4.8	▼2.6	4.8	▼1.2	3.2		
DTD	1.00	1.00	47	127M	25.7	44.3	▲17.8	0.0	▲16.3	0.0	▲19.6	0.0	60.3	▲31.8	0.0	▲27.3	0.0	▲28.4	0.0		
TinyImgNet	1.00	1.00	200	1.2G	57.2	57.8	▲1.9	0.0	▼0.9	0.0	▼1.8	0.0	57.6	▲4.4	0.0	▲2.5	0.0	▲4.7	0.0		
StanfordCars	2.83	0.999	196	481M	49.3	59.6	▲9.9	0.0	▲13.8	2.5	▲5.4	0.0	77.1	▲22.4	0.0	▲28.8	0.0	▲18.2	0.0		
ImageNet	1.00	1.00	1000	3.7G	66.1	62.4	▲5.8	6.2	▲7.0	5.0	▲5.4	3.1	51.0	▼2.5	0.0	▼2.6	0.0	▼3.4	0.0		
SUN397	37.7	0.953	397	146G	55.3	62.5	▲12.9	0.9	▲14.2	0.9	▲13.0	0.9	45.2	▼4.2	7.3	▼2.4	7.3	▼0.2	3.9		
MNIST	1.00	1.00	10	338M	99.5	62.7	▲6.4	5.8	▲7.3	4.7	▲6.2	2.9	92.1	▼0.7	4.4	▼0.5	0.0	▼0.8	0.0		
CIFAR100	1.00	1.00	100	73.6G	69.2	64.2	▲2.2	0.0	▲3.4	0.0	▲1.0	0.0	67.6	▲0.3	0.0	▲4.6	0.0	▼1.0	0.0		
Flowers102	1.00	1.00	102	676M	31.0	66.5	▲15.2	0.0	▲12.7	0.0	▲17.7	0.0	78.0	▼2.4	10.0	▲2.6	0.0	▲0.7	0.0		
Caltech101	86.5	0.902	101	324M	68.8	81.6	▲12.7	0.0	▲14.1	0.0	▲11.3	0.0	88.3	▼5.5	0.0	▼0.1	0.0	▼1.7	0.0		
CIFAR10	1.00	1.00	10	340M	92.9	86.7	▲0.5	0.0	▲2.3	1.1	▲0.6	0.0	86.3	▲1.6	3.3	▲3.4	3.3	▲1.6	3.3		
OxfordIIITPet	1.14	1.00	37	1.6G	26.6	87.3	▲1.9	2.9	▲5.4	2.9	▲4.5	2.9	8.6	▲0.1	0.0	▲1.1	0.0	▲0.8	0.0		
Food101	1.00	1.00	101	5																	

Table 12. Full Component Ablation Study. Impact of removing Online Update, Prototype Refinement, and Skewness Correction on two datasets. Best results under each case are presented with optimal hyperparameters.

Datasets →		CIFAR100								GTSRB									
		Baseline		w/o Online		w/o Skewness		w/o Prototype		Baseline		w/o Online		w/o Skewness		w/o Prototype			
Ablation Cases →	Attack ↓	CA	ASR	CA	ASR	CA	ASR	CA	ASR	CA	ASR	CA	ASR	CA	ASR	CA	ASR		
		Classic	BadNets	72.3	▲2.2	0.0	73.2	▲3.1	5.0	72.1	▲1.9	0.0	70.4	▲0.3	1.0	95.9	▼2.6	0.0	
Backdoor	Blend	73.2	▲2.3	0.0	69.8	▼1.1	6.3	72.9	▲2.0	0.0	71.6	▲0.7	1.0	93.0	▼5.5	2.5	91.3	▼7.2	24.6
	WaNet	68.1	▲4.3	0.0	68.5	▲4.7	4.0	69.4	▲5.6	3.0	67.7	▲4.0	6.1	87.0	▼11.6	0.8	90.2	▼8.4	26.1
Dynamic	BPP	70.4	▲5.6	0.0	68.3	▲3.5	5.5	70.2	▲5.4	0.0	68.5	▲3.7	2.0	95.7	▼0.7	0.0	89.3	▼7.1	19.7
Backdoor	IAB	70.5	▲5.5	0.0	70.6	▲5.6	3.6	70.3	▲5.4	0.0	68.3	▲3.4	0.0	95.7	▼2.6	0.0	91.2	▼7.1	15.0
	SSBA	72.7	▲2.5	0.0	74.3	▲4.1	3.0	72.4	▲2.2	0.0	70.2	▲0.0	0.0	90.0	▼8.3	7.6	80.9	▼17.4	23.2
Clean-Label	CTRL	72.8	▲2.5	0.0	72.9	▲2.6	4.3	72.6	▲2.2	0.0	70.5	▲0.1	0.0	93.1	▼5.5	6.7	91.3	▼7.3	40.2
Backdoor	SIG	72.8	▲2.5	0.0	69.8	▼0.5	5.6	72.5	▲2.2	0.0	71.1	▲0.8	1.0	92.5	▼5.9	0.8	83.9	▼14.5	14.9
	LC	74.0	▲2.7	0.0	73.4	▲2.1	5.4	73.7	▲2.4	0.0	71.9	▲0.6	1.0	92.0	▼6.3	9.9	89.3	▼9.0	38.3
Clean-Image	FLIP	69.9	▼0.2	0.0	66.4	▼3.6	9.1	68.7	▼1.4	0.0	68.7	▼1.4	8.1	92.1	▼3.5	2.4	94.2	▼1.4	3.6
Backdoor	GCB	68.3	▼1.9	2.0	71.5	▲1.3	3.4	67.9	▼2.3	2.0	69.0	▼1.2	3.0	88.5	▼8.8	6.7	76.4	▼20.9	13.5
Average →		71.4	▲2.6	0.2	70.8	▲2.0	5.0	71.1	▲2.3	0.5	69.8	▲1.0	2.1	92.3	▼5.6	3.4	87.9	▼10.0	23.7